Spatially-Distributed RISs vs Relay-Assisted Systems: A Fair Comparison

JIA YE (Student Member, IEEE), ABLA KAMMOUN (Member, IEEE), AND MOHAMED-SLIM ALOUINI (Fellow, IEEE)

Computer Electrical and Mathematical Sciences and Engineering Division, Department of Electrical Engineering,
King Abdullah University of Science and Technology, Thuwal 23955-6900, Saudi Arabia

CORRESPONDING AUTHOR: A. KAMMOUN (e-mail: abla.kammoun@kaust.edu.sa)

ABSTRACT This paper aims to make a comparison between decode-and-forward (DF) relays and reconfigurable intelligent surfaces (RISs) in the case where only one relay or RIS is selected based on the maximization of the signal-to-noise-ratio (SNR). Our study accounts for the spatial distribution of RISs and relays, which is assumed to follow a Poisson point process (PPP). It considers two different path loss models corresponding to RIS/relays randomly located in the near-field and the far-field of the transmitter. Based on the Gamma distribution moment matching method and tools from stochastic geometry, we derive approximations for the outage probability (OP) as well as the energy efficiency (EE) of the RISs-assisted system in the near-field and the far-field scenarios separately. Under the same conditions as RIS, the expressions for OP and EE of the half-duplex and the full-duplex DF relays-assisted systems are also derived. Simulation results are presented to corroborate the proposed analysis and compare between the three technologies. Our results show that RIS is the best choice in the near-field case, regardless of the OP or EE criterion. Compared to half-duplex relays and full-duplex relays, the RIS based system is the most energy-efficient solution to assist communication. Moreover, RIS allows for an improvement in both OP and EE when equipped with more reflecting elements or more densely deployed.

INDEX TERMS Decode-and-forward relays, energy efficiency, far-field, near-filed, outage probability, reconfigurable intelligent surfaces, Poisson point process.

I. INTRODUCTION

AS THE 5G standard is starting its implementation phase, it is critical to look for new communication technologies catering to the ever-increasing demand for traffic rate [1] in the future 5G beyond or even 6G generation. Reconfigurable intelligent surfaces (RISs) are now considered among the key enabling technologies for 6G systems. Empowered by the recent advances in meta-material [2], RISs are equipped with a large number of low-cost passive elements that allow for the modification of the radio waves, in that they reflect, refract, and scatter radio signals in a controllable fashion to counteract the destructive effect of multipath fading. These features can be leveraged to transform the propagation environment into a smart space that can be programmable for the benefit of the communication application. An important research effort is now being devoted to develop hardware architectures based on this technology [3], [4], and to study other related aspects such as channel modeling [5]–[7] and channel estimation [8]–[10], to name a few. Similar to any other technologies, the design of the RIS has been proposed to respond to a variety of criteria such as controlling the signal strength [11], expanding wireless coverage [12], optimizing system capacity [13], [14], maximizing signal-to-interference-ratio [9], minimizing symbol error rate [15], [16], improving physical layer security [17] and increasing energy efficiency (EE) [18].

Recently, an important research effort from both industry and academia has been made to assess the benefits of RIS technology, by carrying out several performance analysis studies [19]–[25]. A major focus has been devoted to theoretical analysis that provides closed-form expressions for several important metrics, such as outage probability (OP) and EE. The advantages of such theoretical studies lie in that they not only avoid the need for extensive numerical simulations but also may assist in finding optimal allocation

resources. Particularly, in [19], approximations for the probability that the channel gain of the backscatter link assisted by RIS exceeds that of the direct link was provided and was shown to match simulation results, while exact closed-form expressions for OP and spectral efficiency were provided in [20] and [21] under reciprocal Rayleigh channels and Fox'H fading channels, respectively. The authors in [23] provide a complete RIS-assisted system performance analysis from the perspective of the instantaneous and average end-to-end signal-to-noise ratio (SNR), the diversity gain, OP, the symbol error rate (SER), the diversity order as well as the ergodic capacity. The closed-form of the ergodic capacity upper bound and OP approximation for the RIS aided single-input single-output (SISO) communication system were derived in [24]. Moreover, the pairwise error probability of a RIS-assisted non-orthogonal multiple access system was analyzed and investigated in [25] assuming imperfect successive interference cancellation, where approximated expression and asymptotic expression are provided.

It is worth mentioning that RISs should not be confused with relay-aided systems or backscatter communication. The main distinguishable feature is that they do not necessitate the use of analog-to-digital/digital-to-analog converters or power amplifiers and ideally can operate at any frequency. Moreover, they can be deployed anywhere, e.g., on the facades of buildings, the ceiling of indoor spaces, or human clothing and furniture. However, like relays, RISs aim to assist communication by enabling higher efficiency gains. This principally motivated the emergence of a series of works aiming to compare between RIS and relay-assisted technologies from outage performance [23] and EE standpoints [26]. In this line, it was shown in [27] that large reflecting elements are needed for the RIS to outperform decode-and-forward (DF) relaying, both in terms of minimizing the total transmit power and maximizing EE, while in [28], it was shown that RIS-assisted single user system is more cost-efficient than amplify-and-forward (AF) relaying. Similarly, an important gain enabled by the use of RIS assisted systems in terms of spatial throughput was also reported in [29] once the number of reflecting elements exceeds a certain value determined by simulation. Moreover, when resource allocation algorithms are used, it was shown in [30] that RIS-assisted systems can achieve 300% higher EE in comparison with the use of regular multi-antenna AF relaying. Following the same line of research, the works in [31], [32] focused on designing optimal and suboptimal schemes to control the consumed power at the network under different settings. More Specifically, the authors in [23] compared the theoretical framework in terms of SNR, OP, SER and ergodic capacity of RIS-assisted system with the one of the corresponding AF relay-assisted system. The comparison results also verified the superiority of RIS.

The current literature has thus far investigated the deployment of only one RIS to support communication. However, in the future, it is expected that these RISs will be densely deployed, and thus transmission will be assisted not only by one RIS but by a multitude of them. This lies behind the motivation of the present work. Particularly, we consider the setting in which communication is assisted by multiple relays and multiple RISs spatially distributed according to a Poisson point process (PPP) [33] in the ring centered at the user. We propose to compare RIS-assisted systems and decode-and-forward (DF) relaying systems of which one RIS/relay is selected based on the maximization of the received SNR. Comparison is carried out in terms of OP and EE and considered both half-duplex and full-duplex relaying systems. Overall, the main differences between our work and the previous works in [23], [27], [30] are:

- Multiple RISs and relays are considered in this work, while only one RIS and one relay are considered in [23], [27], [30]. The selection combining (SC) scheme is also adopted in this work to improve the system performance.
- We account for the spatial distribution of RISs and Relays in this work, which we model by PPP. Under this situation, the distances between base station (BS) and RISs/relays are random, leading to varying path loss and making the system more practical.
- Moreover, our study investigates both near-field and far-field communications, for which expressions for the OP and EE have been provided, while most existing literature investigates only the performance of far-field communications.
- Given that RISs operate in full-duplex mode, we carry out a performance comparison with full-duplex relaying systems in addition to half-duplex relaying systems. Such a comparison is more comprehensive and allows us to draw more insights than its predecessors in the literature.

To pave the way towards a fair comparison of this system, closed-form expressions for OP and EE are derived by leveraging tools from stochastic geometry. Simulations are then carried out to confirm the accuracy of the analytical results and to draw a fair comparison between both systems. Particularly, we confirm that RIS assisted systems compares favorably with both half-duplex and full-duplex assisted systems. Moreover, higher gains can be reaped from this technology when it is equipped with more elements or densely deployed.

The rest of the paper is organized as follows: In Section II, the system model is described. Section III analyzes the performance of RIS-assisted systems in terms of OP and EE, while in Section IV, a theoretical performance analysis for relay-assisted systems is presented. In Section V, some asymptotic results are derived. Some selected discussions about the performance analysis under more practical assumptions are provided in Section VI. Finally, a set of numerical results comparing both systems are provided in Section VII, and conclusions of this paper are drawn in Section VIII.

Table 1 presents the main notions adopted in the following part of this work.

TABLE 1. Notions

Variable	The definition
N	The number of reflecting elements
L	The length of each reflecting elements
f	The carrier frequency
λ	The wavelength
R_1	The inner radius of the circle
R_2	The outer radius of the circle
ρ	The PPP distribution density
P_t/P_r	The transmitted power at the user/relays
P_B/P_U	Power consumption at the BS/user
P_b	Power consumption at eact element at RIS
P_H	dissipated power at each antenna of half-duplex relay
P_F	dissipated power at each antenna of full-duplex relay
ξ	The efficiency of the transmit power amplifier
N_0	The variance of the noise
$d_{m,1}$	The distance between user and m-th RIS
$d_{m,2}$	The distance between RIS and BS
r_U	The distance between user and BS
d_n	The distance between reflecting element n to the center of RIS.
η_1/η_2	The path loss factor for the first/second hop.
η_d	The path loss factor for the direct user-BS link.
$\phi_{m,n}$	The reflecting phase shift of n-th reflecting element at m-th RIS
$\theta_{m,n}/\alpha_{m,n}$	The channel phase shift/amplitude between the user and n-th reflecting element at m-th RIS
$\varphi_{m,n}/\beta_{m,n}$	The channel phase shift/amplitude between the n-th reflecting element at m-th RIS and BS
$h_{m,n}$	The channel between the user and n-th reflecting element at m-th RIS
$g_{m,n}$	The channel between the n-th reflecting element at m-th RIS and BS
$\gamma_{m,N}/\gamma_{m,F}$	The SNR at BS assisted by m-th RIS under the near-field/far-field communication
$\gamma_{RIS,N}/\gamma_{RIS,F}$	The end-to-end SNR assisted by RIS under the near-field/far-field communication
γ_{mB}	The SNR between the m-RIS and BS
$\gamma_{Um,N}/\gamma_{Um,F}$	The SNR between the user and m-RIS in near-field/far-field communication
$\gamma_{DF,N}/\gamma_{DF,F}$	The end-to-end SNR assisted by DF relay under the near-field/far-field communication
γ_{th}	The SNR threshold
$\bar{R}$	The target capacity
$W_R/W_{R,N}/W_{R,F}/W_D/W_{D,N}/W_{D,F}$	Parameter of Chebyshev-Gauss quadrature

FIGURE 1. System model.

II. SYSTEM MODEL

We consider a scenario in which a user communicates through a multiple RIS-assisted system with a single antenna BS. The BS is 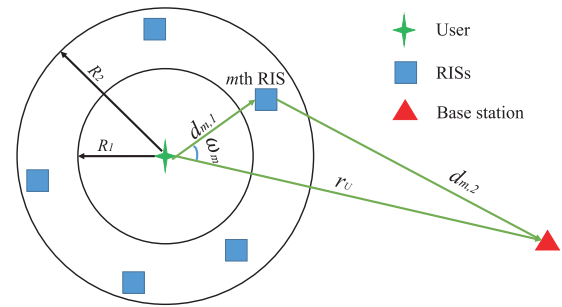located far from the user while the direct link is blocked and as such is ignored. All RISs are composed of $N = N_x \times N_y$ passive and low-cost reflecting elements installed on the wall of a surrounding high-rise building. We assume each RIS to be composed of elements with size $L \times L$ equally spaced on a $N_x \times N_y$ grid. As shown in Fig. 1, RISs are assumed to be spatially distributed according to a homogeneous PPP with density ρ in a circle centered at the user with inner radius R_1 and outer radius R_2. For the sake of simplicity, the planar array of the RIS is perpendicular to the direction of the propagation from the user and that the user, while the centers of all RIS and BS are in the same plane.[1] We consider both near-field and far-field communication[2] between the RISs and the user, which are distinguished by the inner radius $R_1 \gg \max\{N_x, N_y\}L$ [26]. More specifically, we assume near-field communication between the RISs and the user when the RISs are located within R_1, and far-field communication when the RISs are located between R_1 and R_2. Specifically, in the far-field scenario, the spherical wave generated by the transmitter can be approximately regarded as a plane wave at the antenna array side when the distance between the transmitter and the center of the RIS is bigger than R_1. Thus, the probability of RISs to be located in the near-field of the user is $P_{\text{near}} = \frac{R_1^2}{R_2^2}$, while the probability of RISs located in the far-field of the user is $P_{\text{far}} = \frac{R_2^2 - R_1^2}{R_2^2}$.

The distance between the user and BS denoted by r_U is fixed. To reduce the complexity and improve the diversity through multiple RISs, the SC scheme [34] is considered, by which the RIS achieving the largest received SNR is always selected. The RIS selection process is conducted

1. The aim of these assumptions is to simplify the calculation of the intervening distances between the user and the RIS and between the RIS and BS. The first assumption facilitates the calculation of the near-field distances in the first hop, while the second one simplifies the calculation of distances in the second hop. Without these assumptions, the distance between all devices is hard to statistically characterize due to the PPP distributed RISs. Although the considered scenario in this work may be thought of as an ideal case, the closed-form analytical expression derivations for the system performance can be performed to yield important insights into the behavior of the intervening parameters.

2. The far-field refers to the propagation range at which the direction and thus the channel gains are approximately the same from all elements in the array to the transmitting/receiving antenna. On the other hand, the near-field is described in this work by considering that the distance between the transmit antenna to the elements vary over the array.

at the BS by comparing the SNRs estimated based on the received pilot signals transmitted from the user and reflected by each RIS. Other complex combining techniques, e.g., maximum ratio combining (MRC), can also be similarly applied and analyzed based on the proposed analytical method. As the combining technique is not the focus of this work, we omit further details of this question. The fading channels between the user and the n-th reflecting element of RIS m and that between the n-th reflecting element of RIS m and BS are denoted by $h_{m,n} = \alpha_{m,n}e^{-J\theta_{m,n}}$ and $g_{m,n} = \beta_{m,n}e^{-J\varphi_{m,n}}$, where $m = 1,\ldots,M, n = 1,\ldots,N$. Let $\mathbf{\Phi}_m = \text{diag}(e^{J\phi_{m,1}},\ldots,e^{J\phi_{m,N}})$ be the phase shifts applied by the m-th RIS. To facilitate analysis, we assume that the phase resolution is infinite [30]. Since the estimation and feedback process is not the focus of this work, we ignore the delay and power consumption for this process and assume perfect channel state information (CSI) at the BS and perfect feedback information to the RIS. More details regarding this question can be found in [35]. In the next subsection, we will discuss the system performance in the near-field and the far-field respectively. Finally, it is worth mentioning that although this work investigates the performance of uplink RIS-assisted system, where signals transmitted from the user to BS, the analytical method and results can also be applied in the downlink RIS-assisted system, due to signals experiencing the same channel fading and path loss. Specifically, the distance between the user and RISs and the distance between RISs and BS in the downlink RIS-assisted system follow the same distribution as the uplink RIS-assisted system.

A. NEAR-FIELD COMMUNICATION

When RISs are distributed within the inner radius R_1, the number of available RISs M_1 is Poisson distributed with probability $\text{Pr}(M_1) = (\mu_1^{M_1}/M_1!)e^{-\mu_1}$, where $\mu_1 = R_1^2\pi\rho$ denotes the mean measure. The instantaneous SNR at BS is given by:

$$\gamma_{m,N} = \frac{P_t \left| \sum_{n=1}^N \frac{\frac{\alpha_{m,n}}{\eta_1} \frac{\beta_{m,n}}{\eta_2}}{d_{m,n,1}^{\frac{2}{2}} d_{m,2}^{\frac{2}{2}}} e^{j(\phi_{m,n}-\theta_{m,n}-\varphi_{m,n})} \right|^2}{P_L N_0}, \quad (1)$$

where P_t is the transmit power, N_0 is the variance of the noise, $P_L = \frac{16\pi^2}{\lambda^2}$, $\lambda = \frac{c}{f}$ is the wavelength, c is the speed of light, f is the carrier frequency, and $d_{m,n,1}$ and $d_{m,2}$ are the distance between the user and reflecting element n of RIS m and that between RIS m and the BS respectively, while η_1 and η_2 denote the path-loss exponents. Since the distance between the user and RISs are less than R_1, the near-field communication with traditional path loss model is assumed. The distance between reflecting element n to the center of RIS m can be calculated as

$$d_n^2 = \left[-L \left\lfloor \frac{N_x}{2} \right\rfloor + L \bmod (n-1, N_x) \right]^2 + \left[L \left\lfloor \frac{N_y}{2} \right\rfloor - L \left\lfloor \frac{n-1}{N_x} \right\rfloor \right]^2. \quad (2)$$

Therefore, $d_{m,n,1}$ can be calculated as

$$d_{m,n,1}^2 = d_{m,1}^2 + d_n^2, \quad (3)$$

where $d_{m,1}$ is the distances between the user and the center of RIS m. We can easily see that the optimal reflection coefficients are $\phi_{m,n} = \theta_{m,n} + \varphi_{m,n}$. In practice, some estimation errors on the channel phases may exist. In this case, the derived results should be thought of as upper bounds on the achieved performances. Under optimal phases, the SNR associated with m-th RIS is:

$$\gamma_{m,N} = \frac{P_t \left(\sum_{n=1}^N \frac{\frac{\alpha_{m,n}}{\eta_1} \frac{\beta_{m,n}}{\eta_2}}{d_{m,n,1}^{\frac{2}{2}} d_{m,2}^{\frac{2}{2}}} \right)^2}{P_L N_0}. \quad (4)$$

Considering that there is no line-of sight between the BS and RISs, as well as between RISs and the user, we assume that $h_{m,n}$ and $g_{m,n}$ are drawn from a standard Gaussian distribution independently, and hence their modulus follow a standard Rayleigh distribution. In other words, $\alpha_{m,n}$ and $\beta_{m,n}$ are independent Rayleigh distributed random variables.[3] Under this assumption, the exact distribution for $S_N = \sum_{n=1}^N \frac{\frac{\alpha_{m,n}}{\eta_1} \frac{\beta_{m,n}}{\eta_2}}{d_{m,n,1}^{\frac{2}{2}} d_{m,2}^{\frac{2}{2}}}$ could not be easily derived. To overcome this issue, we propose to approximate it with a Gamma distribution, whose shape and sacle parameters are tuned based on the moment matching technique [19], [20]. This technique stands out among many different techniques for approximating non-tractable distributions [36]. Pursing the moment matching technique, the following Lemma gives the Gamma approximation for the probability density function (PDF) and cumulative distribution function (CDF) of S_N.

Lemma 1: The distribution of S_N conditioned on $d_{m,1}$ and $d_{m,2}$ can be approximated with a Gamma distribution whose PDF and CDF are given by:

$$f_{S_N}(x|d_{m,1}, d_{m,2}) = x^{\Psi_N(d_{m,1},d_{m,2})-1} e^{-\frac{x}{\Theta_N(d_{m,1},d_{m,2})}}$$
$$\times \frac{1}{\Gamma(\Psi_N(d_{m,1},d_{m,2}))\Theta_N(d_{m,1},d_{m,2})^{\Psi_N(d_{m,1},d_{m,2})}}, \quad (5)$$

and

$$F_{S_N}(x|d_{m,1}, d_{m,2}) = \frac{\gamma\left(\Psi_N(d_{m,1},d_{m,2}), \frac{x}{\Theta_N(d_{m,1},d_{m,2})}\right)}{\Gamma(\Psi_N(d_{m,1},d_{m,2}))}, \quad (6)$$

where

$$\Psi_N(d_{m,1}, d_{m,2}) = \frac{\left(\sum_{n=1}^N \frac{\pi}{4 d_{m,n,1}^{\frac{\eta_1}{2}} d_{m,2}^{\frac{\eta_2}{2}}} \right)^2}{\sum_{n=1}^N \frac{1-\frac{\pi^2}{16}}{d_{m,n,1}^{\eta_1} d_{m,2}^{\eta_2}}} \quad \text{and} \quad (7)$$

---

3. For the sake of simplicity, we restrict ourselves to the case in which all channels are independent. However, our approach based on the Gamma approximation can handle the case of correlated channels. Indeed, if a correlation model was provided, it would be possible to compute the expectation and variance of S_N, which could be then used to determine the shape and scale of the Gamma distribution.

$$\Theta_N\big(d_{m,1}, d_{m,2}\big) = \frac{\sum_{n=1}^{N} \frac{1-\frac{\pi^2}{16}}{d_{m,n,1}^{\eta_1} d_{m,2}^{\eta_2}}}{\sum_{n=1}^{N} \frac{\pi}{4 d_{m,n,1}^{\frac{\eta_1}{2}} d_{m,2}^{\frac{\eta_2}{2}}}} \qquad (8)$$

represent the shape parameter and scale parameter of Gamma distribution, respectively, $\Gamma(\cdot)$ and $\gamma(\cdot, \cdot)$ are the Gamma function and the incomplete Gamma function defined in [37, (8.310.1), (8.350.1)].

Proof: The proof of **Lemma 1** is provided in Appendix A. ∎

The accuracy of the Gamma approximation was verified in Section VII. Based on **Lemma 1**, the CDF of the SNR can be derived as:

Corollary 1: The CDF of SNR associated with m-th RIS $\gamma_{m,N} = \frac{P_t S_N^2}{P_L N_0}$ can be expressed as

$$F_{\gamma_{m,N}}\big(x|d_{m,1}, d_{m,2}\big) = \frac{1}{\Gamma\big(\Psi_N\big(d_{m,1}, d_{m,2}\big)\big)}$$
$$\times \gamma\left(\Psi_N\big(d_{m,1}, d_{m,2}\big), \frac{\sqrt{x}}{\sqrt{\bar{\gamma}}\Theta_N\big(d_{m,1}, d_{m,2}\big)}\right), \qquad (9)$$

where $\bar{\gamma} = \frac{P_t}{P_L N_0}$.

Proof: The distribution of $\gamma_{m,N} = \bar{\gamma} S_N^2$ can be obtained easily through variable substitution based on the distribution of S_N shown in (6). ∎

B. FAR-FIELD COMMUNICATION

For the far-field case, RISs are located within the ring with inner radius R_1 and outer radius R_2. The number of available RISs M_2 is Poisson distributed with probability $\Pr(M_2) = (\mu_2^{M_2}/M_2!)e^{-\mu_2}$, where $\mu_2 = (R_2^2 - R_1^2)\pi\rho$ denotes the mean measure. In this case, the distances between the user or the BS and each element of the RIS can be approximated to be same. Thus, the instantaneous SNR with optimal phase shifts at BS is given by:

$$\gamma_{m,F} = \frac{P_t \left| \sum_{n=1}^{N} \alpha_{m,n}\beta_{m,n} \right|^2}{d_{m,1}^{\eta_1} d_{m,2}^{\eta_2} P_L N_0}. \qquad (10)$$

Similar to the near-field, We firstly derive the distribution of $S_F = \sum_{n=1}^{N} \alpha_{m,n}\beta_{m,n}$ in the following lemma and then derive the CDF of $\gamma_{m,F}$ accordingly.

Lemma 2: The distribution of S_F conditioned on $d_{m,1}$ and $d_{m,2}$ can be approximated with a Gamma distribution which has the PDF and CDF

$$f_{S_F}\big(x|d_{m,1}, d_{m,2}\big) = \frac{x^{\Psi_F - 1} e^{-\frac{x}{\Theta_F}}}{\Gamma(\Psi_F)\Theta_F^{\Psi_F}}, \qquad (11)$$

and

$$F_{S_F}\big(x|d_{m,1}, d_{m,2}\big) = \frac{\gamma\left(\Psi_F, \frac{x}{\Theta_F}\right)}{\Gamma(\Psi_F)}, \qquad (12)$$

where $\Psi_F = \frac{N\pi^2}{16-\pi^2}$ and $\Theta_F = \frac{16-\pi^2}{4\pi}$ represent the shape parameter and scale parameter of Gamma distribution, respectively.

Proof: The expectation and variance of S_F conditioned on $d_{m,1}$ and $d_{m,2}$ are $\mathbb{E}[S_F|d_{m,n,1}, d_{m,2}] = \frac{N\pi}{4}$ and $\mathrm{var}[S_F|d_{m,n,1}, d_{m,2}] = N(1 - \frac{\pi^2}{16})$. Based on the moment matching method, we find the parameters of the Gamma distribution that has the same mean and variance as S_F. The expectation and variance of a Gamma distribution with shape parameter Ψ_F and scale parameter Θ_F are $\Psi_F \Theta_F$ and $\Psi_F \Theta_F^2$, respectively. We thus obtain the following system of two equation for Ψ_F and Θ_F: $\Psi_F \Theta_F = \frac{N\pi}{4}$ and $\Psi_F \Theta_F^2 = N(1 - \frac{\pi^2}{16})$, from which we can easily deduce $\Psi_F = \frac{N\pi^2}{16-\pi^2}$, $\Theta_F = \frac{16-\pi^2}{4\pi}$. Therefore, according to the moment matching method, the distribution of $S_F = \sum_{n=1}^{N} \alpha_{m,n}\beta_{m,n}$ can be approximated by a Gamma distribution with shape parameter Ψ_F and scale parameter Θ_F. ∎

Similarly to the near-field communication, we derive the CDF for $\gamma_{m,F}$ as:

Corollary 2: The CDF of γ_m conditioning on $d_{m,1}$ and $d_{m,2}$ can be expressed as:

$$F_{\gamma_{m,F}}\big(x|d_{m,1}, d_{m,2}\big) = \frac{1}{\Gamma(\Psi_F)} \gamma\left(\Psi_F, \Omega\sqrt{x d_{m,1}^{\eta_1} d_{m,2}^{\eta_2}}\right), \qquad (13)$$

where $\Omega = \sqrt{\frac{1}{\bar{\gamma}\Theta_F^2}}$.

Proof: The distribution of $\gamma_{m,F} = \frac{\bar{\gamma}S_F^2}{d_{m,1}^{\eta_1} d_{m,2}^{\eta_2}}$ can be obtained easily through variable substitution based on the distribution of S_F shown in (12). ∎

III. RISS-ASSISTED SYSTEM PERFORMANCE ANALYSIS

In this section, we analyze the system performance in terms of OP and EE for the RISs-assisted system in the near-field and the far-field cases separately. We assume that a SC scheme is adopted by which the BS chooses the RIS that achieves the maximum end-to-end SNR to assist communication.

A. OUTAGE PERFORMANCE

The overall received SNR based on the SC scheme could be derived as $\gamma_{RIS} = \max_{m\in\mathcal{S}}\{\gamma_m\}$, where $\mathcal{S}$ denotes the set of PPP distributed RISs in the ring. From Fig. 1, the relationship between $d_{m,1}$ and r_U is $d_{m,2} = \sqrt{d_{m,1}^2 + r_U^2 - 2d_{m,1} r_U \cos\omega_m}$, where r_U is the fixed distance from the user to BS and ω_m is the randomly distributed angle between the direct link and the first reflect link. Since $d_{m,2}$ is function of $d_{m,1}$ and ω_m, the CDF of the overall SNR conditioned on $d_{m,1}$ and ω_m at the BS is $F_{\gamma_{RIS}}(x|d_{m,1}, \omega_m) = \prod_{m\in\mathcal{S}} F_{\gamma_m}(x|d_{m,1}, \omega_m)$. Hence, the CDF associated with the SNR is given as

$$F_{\gamma_{RIS}}(x) = \mathbb{E}_{d_{m,1}, \omega_m}\left[\prod_{m\in\mathcal{S}} F_{\gamma_m}\big(x|d_{m,1}, \omega_m\big) \right]$$
$$= \exp\left\{ -\int_{\mathcal{S}} \rho\big[1 - F_{\gamma_m}\big(x|d_{m,1}, \omega_m\big)\big]\mathrm{d}d_{m,1}\mathrm{d}\omega_m \right\}, \qquad (14)$$

and $\mathbb{E}_{d_{m,1},\omega_m}$ denotes the expectation with respect to the random variables $d_{m,1}$ and ω_m. The above integral is hard to solve for both near-field and far-field communication scenarios. The difficulty stems from the randomness of $d_{m,2}$ which is not easy to handle. To overcome this issue, we assume from now on that the outer radius of the ring is much smaller than the distance between the user and the BS, which allows us to approximate $d_{m,2}$ by r_U.

1) NEAR-FIELD COMMUNICATION

Lemma 3: Assuming RISs are PPP distributed in the inner circle, we obtain $F_{\gamma_{RIS,N}}(x)$ as (15) shown on the bottom of the page, where $w_R = \frac{\pi}{W_R}$, $\vartheta_i = \cos(\frac{2i-1}{2W_R}\pi)$.

Proof: The proof of **Lemma 3** is provided in Appendix B. ∎

As a consequence, the OP of the proposed system can be shown as $P_{out,N} = \Pr\{\gamma_{RIS,N} \leq \gamma_{th}\} = F_{\gamma_{RIS,N}}(\gamma_{th})$, where γ_{th} is the threshold value.

2) FAR-FIELD COMMUNICATION

Lemma 4: Assuming RISs are PPP distributed in the outer circle, we obtain $F_{\gamma_{RIS,F}}(x)$ as

$$F_{\gamma_{RIS,F}}(x) = \exp\{\zeta_1 + \zeta_2[\mathcal{F}_I(R_2, \Omega, x) - \mathcal{F}_I(R_1, \Omega, x)]\},$$
(16)

where $\zeta_1 = -\pi\rho(R_2^2 - R_1^2)$, $\zeta_2 = \frac{4\pi\rho}{\eta_1\Gamma(\Psi_F)}$, $\mathcal{F}_I(R_i, \Omega, x) = R_i^2 G_{23}^{12}\left(\Omega\sqrt{xR_i^{\eta_1}r_U^{\eta_2}}\,\middle|\,\begin{matrix}1, 1-\frac{4}{\eta_1}\\\Psi_F, -\frac{4}{\eta_1}, 0\end{matrix}\right)$ with $i = 1, 2$.

Proof: Using the representation of the incomplete Gamma function in terms of Meijer's G-Function in [38, 8.4.16.1] and approximating $d_{m,2}$ by r_U, the CDF of $\gamma_{m,F}$ conditioning on $d_{m,1}$ is given by:

$$F_{\gamma_{m,F}}(x|d_{m,1}) = \frac{1}{\Gamma(\Psi_F)} G_{12}^{11}\left(\Omega\sqrt{xd_{m,1}^{\eta_1}r_U^{\eta_2}}\,\middle|\,\begin{matrix}1\\\Psi_F, 0\end{matrix}\right).$$
(17)

Then, applying (14) to (9), we calculate $F_{\gamma_{RIS,F}}(x)$ as

$$F_{\gamma_{RIS,F}}(x) = \exp\left\{-\rho\int_{R_1}^{R_2}\int_0^{2\pi} r\right.$$
$$\times \left[1 - \frac{1}{\Gamma(\Psi_F)}G_{12}^{11}\left(\Omega\sqrt{xr^{\eta_1}r_U^{\eta_2}}\,\middle|\,\begin{matrix}1\\\Psi_F, 0\end{matrix}\right)\right]\mathrm{d}r\mathrm{d}\theta\right\}$$
$$= \exp\left\{-\pi\rho\left(R_2^2 - R_1^2\right) + 2\pi\rho\int_{R_1^{\frac{\eta_1}{2}}}^{R_2^{\frac{\eta_1}{2}}} \frac{t^{\frac{4}{\eta_1}-1}}{\Gamma(\Psi_F)}\right.$$
$$\times \left. G_{12}^{11}\left(\Omega\sqrt{xr_U^{\eta_2}}t\,\middle|\,\begin{matrix}1\\\Psi_F, 0\end{matrix}\right)\mathrm{d}t\mathrm{d}\theta\right\}.$$
(18)

By using [39, Eq. (26)], the expression of $F_{\gamma_{RIS,F}}(x)$ can be finally expressed as (16). This completes the proof of **Lemma 4**. ∎

Hence, the OP of the end-to-end SNR in the far-field communication scenario is given by $P_{out,F} = F_{\gamma_{RIS,F}}(\gamma_{th})$.

B. ENERGY EFFICIENCY

The EE is defined as $\eta = \frac{BR}{P_{\text{total}}}$ where B is the transmission bandwidth, R is the achievable capacity in *bps* and P_{total} is the total power consumption in Joule. The total power consumption of the RIS-assisted system is $P_{RIS} = \xi^{-1}P_t + P_B + P_U + NP_b$ [27], where ξ is the efficiency of the transmit power amplifier, P_B and P_U denote the hardware-dissipated power consumption at the user and BS, P_b is the power consumed by each element at RIS.

1) NEAR-FIELD COMMUNICATION

Lemma 5: The EE of RIS-assisted system in near-field can be approximated by (19) shown at the bottom of the page, where $P_R = P_B + NP_b + P_U$, $\Lambda_R = \frac{2^{\tilde{R}}-1}{\xi}$ and $\Xi_R = \frac{B\tilde{R}\Lambda_R}{P_R}$, $\tilde{\gamma} = P_L N_0$, $w_{R,F} = \frac{\pi}{W_{R,F}}$, $w_{R,N} = \frac{\pi}{W_{R,N}}$, $g_{j,N} = \cos(\frac{2j-1}{2W_{R,N}}\pi)$ and $\epsilon_{j,N} = \frac{g_{j,N}+1}{2\Lambda_R}$.

Proof: The proof of **Lemma 5** is provided in Appendix C. ∎

$$F_{\gamma_{RIS,N}}(x) \approx \exp\left\{-\pi\rho R_1^2 + \pi\rho R_1 \sum_{i=1}^{W_R} w_R\sqrt{1-\vartheta_i^2}\frac{\frac{R_1(\vartheta_i+1)}{2}}{\Gamma\left(\Psi_N\left(\frac{R_1(\vartheta_i+1)}{2}\right)\right)}\gamma\left(\Psi_N, \frac{\sqrt{x}}{\sqrt{\bar{\gamma}}\Theta_N\left(\frac{R_1(\vartheta_i+1)}{2}\right)}\right)\right\}$$
(15)

$$\eta_{RIS,N} \approx \frac{B\tilde{R}}{P_{EI}} - \Xi_R \sum_{j=1}^{W_{R,N}} w_{R,N}\sqrt{1-g_{j,N}^2}\exp\left\{-\pi\rho R_1^2 + \pi\rho\sum_{i=1}^{W_R}\frac{w_R\sqrt{1-\vartheta_i^2}R_1(\vartheta_i+1)}{\Gamma\left(\Psi_N\left(\frac{R_1(\vartheta_i+1)}{2}\right)\right)}\gamma\left(\Psi_N, \frac{\sqrt{\tilde{\gamma}\left(\frac{1}{\epsilon_{j,N}P_R} - \frac{\Lambda_R}{P_R}\right)}}{\Theta_N\left(\frac{R_1(\vartheta_i+1)}{2}\right)}\right)\right\}$$
(19)

2) FAR-FIELD COMMUNICATION

Lemma 6: Based on the distribution of $\gamma_{RIS,F}$, we can obtain EE for far-field as

$$
\begin{aligned}
\eta_{RIS,F} \approx \frac{B\bar{R}}{P_R} - \sum_{j=1}^{W_{R,F}} w_{R,F} \sqrt{1 - g_{j,F}^2} \frac{\Xi_R}{2\Lambda_R} \\
\times \exp\Bigg\{ \zeta_1 + \zeta_2 \Bigg[\mathcal{F}_I\bigg(R_2, \sqrt{\frac{N_0}{\Theta_F^2}}, \bigg(\frac{1}{\epsilon_{j,F}P_R} - \frac{\Lambda_R}{P_R}\bigg)\bigg) \\
- \mathcal{F}_I\bigg(R_1, \frac{\sqrt{\bar{\gamma}}}{\Theta_F}, \bigg(\frac{1}{\epsilon_{j,F}P_R} - \frac{\Lambda_R}{P_R}\bigg)\bigg) \Bigg] \Bigg\},
\end{aligned}
$$
(20)

where $g_{j,F} = \cos(\frac{2j-1}{2W_{R,F}}\pi)$ and $\epsilon_{j,F} = \frac{g_{j,F}+1}{2\Lambda_R}$.

Proof: Similarly, defining $\gamma'_{RIS,F} = \max_{m\in\mathcal{S}}\left\{ \frac{|\sum_{n=1}^{N}\alpha_{m,n}\beta_{m,n}|^2}{d_{m,1}^{\eta_1}d_{m,2}^{\eta_2}P_L N_0} \right\}$ and using the expression $P_t = \frac{2^{\bar{R}}-1}{\mathbb{E}[\gamma'_{RIS,F}]}$, the EE in far-field can re-expressed through the same way shown in Appendix C as:

$$
\eta_{RIS,F} = \frac{B\bar{R}}{P_R} - \Xi_R \mathbb{E}\left[\frac{1}{\Lambda_R + P_R \gamma'_{RIS,F}} \right].
$$
(21)

Also, using the relation $\mathbb{E}_X(x) = \int_0^\infty \Pr\{X > t\}dt$, we can have

$$
\mathbb{E}\left[\frac{1}{\Lambda_R + P_R\gamma'_{RIS,F}} \right] = \int_0^{\frac{1}{\Lambda_R}} \Pr\left\{ \gamma'_{RIS,F} < \frac{1}{tP_R} - \frac{\Lambda_R}{P_R} \right\}dt.
$$
(22)

The approximated expression of $\eta_{RIS,F}$ can be obtained using the Chebyshev-Gauss quadrature approximation. ∎

IV. COMPARISON WITH RELAY-ASSISTED SYSTEMS

In this section, we analyze the system performance when the RIS are replaced by DF relays to assist communication. For the sake of fairness, we assume that DF relays are geometrically placed and distributed as the RISs, and are equipped similarly to RIS with N receive and transmit antennas while employing MRC. Similar to the RIS-assisted system, the SC scheme is also adopted in the relay-assisted system and consists in selecting the relay achieving the largest received SNR to assist the transmission. Under this setting, we compare the OP and EE in near-field and far-field scenarios with those obtained by the RIS assisted system. Both half-duplex and full-duplex relaying will be considered.

A. HALF-DUPLEX RELAY-ASSISTED SYSTEM
1) OUTAGE PERFORMANCE

Near-Field Communication: The received SNR at the m-th relay and the BS can be expressed as $\gamma_{Um,N} = \frac{P_t|\mathbf{h}_{Um,N}|^2}{P_L N_0}$ and $\gamma_{mB} = \frac{P_r|\mathbf{h}_{mB}|^2}{d_{m,2}^{\eta_2}P_L N_0}$, where $\mathbf{h}_{Um,N} \in \mathbb{C}^N$ accounts for both the path-loss and small-sacle fading between the m-th DF relay and the user, with each entry following

Gaussian distribution with zero mean and variance $\frac{1}{d_{m,n,1}^{\eta_1}}$, and $\mathbf{h}_{mB} \in \mathbb{C}^N$ denotes the channel between m-th DF relay and BS and follows a standard normal distribution. Based on the CSI of both links, the optimal source-relay-destination link (OSRDL) is selected [40]. Its SNR is given by $\gamma_{DF} = \max_{m\in\mathcal{S}}\{\min\{\gamma_{Um,N}, \gamma_{mB}\}\}$. Considering MRC at each relay, the CDF of $\gamma_{Um,N}$ conditioned on $d_{m,1}$ can be given by [41] as

$$
F_{\gamma_{Um,N}}(x|d_{m,1}) = 1 - \mathbf{e}^T \exp\left(\sqrt{\frac{x}{\bar{\gamma}}}\mathbf{A}_1(d_{m,1})\right)\mathbf{e}_1, \quad (23)
$$

where $\mathbf{e} = [1, 0, \ldots, 0]^T \in \mathbb{R}^{N\times 1}$, $\mathbf{e}_1 = [1, 1, \ldots, 1]^T \in \mathbb{R}^{N\times 1}$, and $\mathbf{A}(d_{m,1})$ is given by

$$
\mathbf{A}(d_{m,1}) = \begin{pmatrix}
-d_{m,1,1}^{\frac{\eta_1}{2}} & d_{m,1,1}^{\frac{\eta_1}{2}} & 0 & \cdots & 0 \\
0 & -d_{m,2,1}^{\frac{\eta_1}{2}} & d_{m,2,1}^{\frac{\eta_1}{2}} & \cdots & 0 \\
\vdots & \vdots & \ddots & \ddots & \vdots \\
0 & \cdots & 0 & 0 & -d_{m,N,1}^{\frac{\eta_1}{2}}
\end{pmatrix},
$$
(24)

while the distribution of γ_{mB} conditioned on $d_{m,2}$ is expressed as

$$
F_{\gamma_{mB}}(x|d_{m,2}) = 1 - \exp\left(-d_{m,2}^{\eta_2}\frac{x}{\bar{\gamma}}\right)\sum_{j=0}^{N-1}\frac{d_{m,2}^{j\eta_2}x^j}{\bar{\gamma}^j j!}. \quad (25)
$$

Thus, the CDF of $\gamma_{UmB,N} = \min\{\gamma_{Um,N}, \gamma_{mB}\}$ conditioning on $d_{m,1}$ and $d_{m,2}$ is

$$
\begin{aligned}
F_{\gamma_{UmB,N}}(x|d_{m,1}, d_{m,2}) = 1 - \mathbf{e}^T \exp\left(\frac{x}{\bar{\gamma}}\mathbf{A}(d_{m,1})\right)\mathbf{e}_1 \\
\times \exp\left(-d_{m,2}^{\eta_2}\frac{x}{\bar{\gamma}}\right)\sum_{j=0}^{N-1}\frac{d_{m,2}^{j\eta_2}x^j}{\bar{\gamma}^j j!}.
\end{aligned}
$$
(26)

Lemma 7: Assuming relays are PPP distributed in the inner circle, the CDF of $\gamma_{DF,N}$ in the near-field communication can be approximated as:

$$
\begin{aligned}
F_{\gamma_{DF,N}}(x) \approx \exp\Bigg\{ -\pi\rho R_1 \sum_{i=1}^{W_D} w_D \sqrt{1 - v_i^2} \exp\left(-r_U^{\eta_2}\frac{x}{\bar{\gamma}}\right) \\
\times \sum_{j=0}^{N-1} \frac{r_U^{j\eta_2}x^j}{\bar{\gamma}^j j!}\frac{R_1(v_i+1)}{2}\mathbf{e}^T \\
\times \exp\left(\frac{x}{\bar{\gamma}}\mathbf{A}\left(\frac{R_1(v_i+1)}{2}\right)\right)\mathbf{e}_1 \Bigg\},
\end{aligned}
$$
(27)

where $w_D = \frac{\pi}{W_D}$, $v_i = \cos(\frac{2i-1}{2W_D}\pi)$.

Proof: Based on the approximation $r_U \approx d_{m,2}$ and applying (14) to (26), the CDF of $\gamma_{DF,N}$ can be calculated as

$$F_{\gamma_{DF,N}}(x) = \exp\left\{ -\rho \int_0^{R_1} \int_0^{2\pi} d_{m,1} \mathbf{e}^T \exp\left(\frac{x}{\tilde{\gamma}} \mathbf{A}(d_{m,1}) \right) \mathbf{e}_1 \right.$$
$$\left. \times \exp\left(-r_U^{\eta_2} \frac{x}{\tilde{\gamma}} \right) \sum_{j=0}^{N-1} \frac{r_U^{j\eta_2} x^j}{\tilde{\gamma}^j j!} d d_{m,1} d\theta \right\}. \tag{28}$$

The proof of **Lemma 7** can be completed through the Chebychev-Gauss quadrature approximation. ∎

The OP of the relay-assisted system for the near-field communication is thus given by $F_{\gamma_{DF,N}}(\gamma_{th})$.

Far-Field Communication: The received SNR at the output of the MRC scheme of the m-th relay in the far-field communication can be expressed as $\gamma_{Um,F} = \frac{P_t |\mathbf{h}_{Um,F}|^2}{P_L N_0}$, where $\mathbf{h}_{Um,F}$ follows a standard Gaussian distribution with mean 0 and covariance $\frac{1}{d_m^{\eta_1}} \mathbf{I}_N$. Therefore, the CDF of $\gamma_{UmB,F} = \min\{\gamma_{Um,F}, \gamma_{mB}\}$ in the far-field scenario conditioning on $d_{m,1}$ and $d_{m,2}$ is given by:

$$F_{\gamma_{UmB,F}}(x|d_{m,1}, d_{m,2}) = 1 - \exp\left(-\frac{x}{\tilde{\gamma}} d_{m,1}^{\eta_1} \right) \sum_{i=0}^{N-1} \frac{d_{m,1}^{i\eta_1} x^i}{\tilde{\gamma}^i i!}$$
$$\times \exp\left(-d_{m,2}^{\eta_2} \frac{x}{\tilde{\gamma}} \right) \sum_{j=0}^{N-1} \frac{d_{m,2}^{j\eta_2} x^j}{\tilde{\gamma}^j j!}. \tag{29}$$

Lemma 8: Assuming relays are PPP distributed in the outer circle, we obtain CDF of $\gamma_{DF,F}$ in the far-field communication as

$$F_{\gamma_{DF,F}}(x) = \exp\left\{ -\frac{2\pi\rho}{\eta_1} \sum_{i=0}^{N-1} \frac{x^{-\frac{2}{\eta_1}}}{\tilde{\gamma}^{-\frac{2}{\eta_1}} i!} \mathcal{F}_R(R_1, R_2, x, i) \right.$$
$$\left. \times \exp\left(-\frac{x}{\tilde{\gamma}} r_U^{\eta_2} \right) \sum_{j=0}^{N-1} \frac{r_U^{j\eta_2} x^j}{\tilde{\gamma}^j j!} \right\}, \tag{30}$$

where $\mathcal{F}_R(R_1, R_2, x, i) = \gamma(\frac{2}{\eta_1} + i, \frac{R_2^{\eta_1} x}{\tilde{\gamma}}) - \gamma(\frac{2}{\eta_1} + i, \frac{R_1^{\eta_1} x}{\tilde{\gamma}})$.

Proof: Based on the approximation $r_U \approx d_{m,2}$ and applying (14) to (29), the CDF of $\gamma_{DF,F}$ can be calculated as

$$F_{\gamma_{DF,F}}(x) = \exp\left\{ -\rho \int_{R_1}^{R_2} \int_0^{2\pi} d_{m,1} \exp\left(-\frac{x}{\tilde{\gamma}} d_{m,1}^{\eta_1} \right) \right.$$
$$\times \sum_{i=0}^{N-1} \frac{d_{m,1}^{i\eta_1} x^i}{\tilde{\gamma}^i i!} \exp\left(-\frac{x}{\tilde{\gamma}} r_U^{\eta_2} \right) \sum_{j=0}^{N-1} \frac{r_U^{j\eta_2} x^j}{\tilde{\gamma}^j j!} d d_{m,1} d\theta \right\}$$
$$= \exp\left\{ -\frac{2\pi\rho}{\eta_1} \int_{R_1^{\eta_1}}^{R_2^{\eta_1}} \exp\left(-\frac{x}{\tilde{\gamma}} y \right) \sum_{i=0}^{N-1} \frac{y^{\frac{2}{\eta_1}+i-1} x^i}{\tilde{\gamma}^i i!} \right.$$

$$\left. \times \exp\left(-\frac{x}{\tilde{\gamma}} r_U^{\eta_2} \right) \sum_{j=0}^{N-1} \frac{r_U^{j\eta_2} x^j}{\tilde{\gamma}^j j!} dy \right\}. \tag{31}$$

By using [37, Eq. (3.381.1)], we can easily derive $F_{\gamma_{DF,F}}(x)$ as (30). ∎

The OP of the relay-assisted system is thus given by $F_{\gamma_{DF,F}}(\gamma_{th})$.

2) ENERGY EFFICIENCY

As compared to a RIS assisted system, the DF relaying system consumes a transmit power P_r at the relay, but it is active half of the time. The power consumed by the DF relay is given by [30], [42]: $P_{DF,H} = \frac{1}{2}[\xi^{-1}(P_r + P_t) + P_B + P_U + NP_H]$. Hence, the EE of the relaying system is $\eta_{DF} = \frac{\frac{1}{2} B \mathbb{E}[\log_2(1+\gamma_{DF})]}{\frac{1}{2}[\xi^{-1}(P_r+P_t)+P_B+P_U+NP_H]}$, where P_H denotes the dissipated power at each half-duplex DF relay transmit-receive antenna. Setting $P_r = P_t$, the transmit power at the user and DF relay that is required to achieve a capacity $\bar{R}$ is:

$$P_t = P_r = \frac{2^{2\bar{R}} - 1}{\max_{m \in \mathcal{S}} \left\{ \min\left\{ \frac{|\mathbf{h}_{Um,i}|^2}{P_L N_0}, \frac{|\mathbf{h}_{mB}|^2}{d_{m,2}^{\eta_2} P_L N_0} \right\} \right\}}, \tag{32}$$

where $i \in \{N, F\}$.

Near-Field Communication:

Lemma 9: Based on the distribution of $\gamma_{DF,N}$, we can obtain EE of relay-assisted system for near-field as

$$\eta_{DF,N} \approx \frac{B\bar{R}}{P_{D,H}} - \mathcal{F}_N(\Lambda_D, \Xi_D, P_{D,H}), \tag{33}$$

where $P_{D,H} = P_B + P_U + NP_F$, $\Lambda_D = \frac{2^{2\bar{R}+1}-2}{\xi}$ and $\Xi_D = \frac{B\bar{R}\Lambda_D}{P_{D,H}}$, $\mathcal{F}_N(\Lambda_D, \Xi_D, P_{D,H})$ is given as

$$\mathcal{F}_N(\Lambda_D, \Xi_D, P_{D,H}) = \sum_{p=1}^{W_{D,N}} w_{D,N} \sqrt{1 - v_{p,N}^2} \frac{\Xi_D}{2\Lambda_D}$$
$$\times \exp\left\{ -\pi\rho R_1 \sum_{i=1}^{W_D} w_D \sqrt{1 - v_i^2} \frac{R_1(v_i + 1)}{2} \mathbf{e}^T \right.$$
$$\times \exp\left(\tilde{\gamma}\left(\frac{2\Lambda_D}{(v_{p,N}+1)P_{D,H}} - \frac{\Lambda_D}{P_{D,H}} \right) \mathbf{A}\left(\frac{R_1(v_i + 1)}{2} \right) \right)$$
$$\times \mathbf{e}_1 \sum_{j=0}^{N-1} \frac{\tilde{\gamma}^j r_U^{j\eta_2} \left(\frac{2\Lambda_D}{(v_{p,N}+1)P_{D,H}} - \frac{\Lambda_D}{P_{D,H}} \right)^j}{j!}$$
$$\left. \times \exp\left(-\tilde{\gamma} r_U^{\eta_2} \left(\frac{2\Lambda_D}{(v_{p,N}+1)P_{D,H}} - \frac{\Lambda_D}{P_{D,H}} \right) \right) \right\}, \tag{34}$$

where $w_{D,N} = \frac{\pi}{W_{D,N}}$, $v_{p,N} = \cos(\frac{2p-1}{2W_{D,N}}\pi)$.

Proof: Denoting $\gamma'_{DF,N} = \max_{m \in \mathcal{S}}\{\min\{\frac{|\mathbf{h}_{Um,N}|^2}{P_L N_0}, \frac{|\mathbf{h}_{mB}|^2}{d_{m,2}^{\eta_2} P_L N_0}\}\}$ and using the expression of P_t and P_r required to obtain fixed capacity $\bar{R}$, the EE can be simplified as:

$$\eta_{DF,N} = \frac{B\bar{R}}{P_{D,H}} - \Xi_D \mathbb{E}\left[\frac{1}{\Lambda_D + P_{D,H} \gamma'_{DF,N}} \right]$$

$$\approx \frac{B\bar{R}}{P_{D,H}} - \Xi_D \int_0^{\frac{1}{\Lambda_D}} \exp\left\{-\pi\rho R_1 \sum_{i=1}^{W_D} w_D \sqrt{1-v_i^2}\right.$$

$$\times \frac{R_1(v_i+1)}{2} \exp\left(-\tilde{\gamma} r_U^{\eta_2}\left(\frac{1}{tP_{D,H}} - \frac{\Lambda_D}{P_{D,H}}\right)\right)$$

$$\times \sum_{j=0}^{N-1} \frac{\tilde{\gamma}^j r_U^{j\eta_2}\left(\frac{1}{tP_{D,H}} - \frac{\Lambda_D}{P_{D,H}}\right)^j}{j!} \mathbf{e}^T$$

$$\left. \times \exp\left(\tilde{\gamma}\left(\frac{1}{tP_{D,H}} - \frac{\Lambda_D}{P_{D,H}}\right) \mathbf{A}_1\left(\frac{R_1(v_i+1)}{2}\right)\right)\mathbf{e}_1\right\}\mathrm{d}t. \tag{35}$$

Using again the Chebyshev-Gauss quadrature approximation to solve the above integral, we can obtain the expression of $\eta_{DF,N}$. ∎

Far-Field Communication:

Lemma 10: Based on the distribution of $\gamma_{DF,F}$, we can obtain EE of relay-assisted system for far-field as

$$\eta_{DF,F} = \frac{B\bar{R}}{P_{D,H}} - \mathcal{F}_F(\Lambda_D, \Xi_D, P_{D,H}), \tag{36}$$

where $\mathcal{F}_F(\Lambda_D, \Xi_D, P_{D,H})$ is given by

$$\mathcal{F}_F(\Lambda_D, \Xi_D, P_{D,H}) = \sum_{p=1}^{W_{D,F}} w_{D,F}\sqrt{1-v_{p,F}^2}\frac{\Xi_D}{2\Lambda_D}$$

$$\times \exp\left\{-\frac{2\pi\rho}{\eta_1}\sum_{i=0}^{N-1}\frac{\left[\tilde{\gamma}\left(\frac{2\Lambda_D}{(v_{p,F}+1)P_{D,H}} - \frac{\Lambda}{P_{D,H}}\right)\right]^{-\frac{2}{\eta_1}}}{i!}\right.$$

$$\times \mathcal{F}_R\left(R_1, R_2, \rho, \left(\frac{2\Lambda_D}{(v_{p,F}+1)P_{D,H}} - \frac{\Lambda_D}{P_{D,H}}\right), i\right)$$

$$\times \exp\left(-\tilde{\gamma} r_U^{\eta_2}\left(\frac{2\Lambda_D}{(v_{p,F}+1)P_{D,H}} - \frac{\Lambda_D}{P_{D,H}}\right)\right)$$

$$\left.\times \sum_{j=0}^{N-1}\frac{\tilde{\gamma}^j r_U^{j\eta_2}\left(\frac{2\Lambda_D}{(v_{p,F}+1)P_{D,H}} - \frac{\Lambda_D}{P_{D,H}}\right)^j}{j!}\right\}, \tag{37}$$

where $w_{D,F} = \frac{\pi}{W_{D,F}}$, $v_{p,F} = \cos(\frac{2p-1}{2W_{D,F}}\pi)$.

Proof: The proof follows along the same lines as in the near-field communication. It is based on setting P_t and P_r as (32) and using the Chebyshev-Gauss quadrature approximation. ∎

B. COMPARISON WITH FULL-DUPLEX RELAY-ASSISTED SYSTEM

Under the same setting as before, we analyze the OP and EE in near-field and far-field scenarios for a full-duplex DF relay-assisted system. For simplicity, we assume perfect relay interference mitigation at each relay. The analysis follows along the same lines as the half-duplex, the only difference being that the rate is twice as the one achieved by the half-duplex and that a certain amount of power

is required to mitigate the inter-relay interference. The power consumed by the full-duplex DF relay is given by: $P_{DF,F} = \xi^{-1}(P_r + P_t) + P_B + P_U + NP_F$, where P_F composed of the consumed hardware-dissipated power and the power used for mitigating self-interference at each transmit-receive antenna of full-duplex DF relay. Hence, the EE of the relaying system is $\eta_{DF,F,i} = \frac{B\mathbb{E}[\log_2(1+\gamma_{DF,i})]}{\xi^{-1}(P_r+P_t)+P_B+P_U+NP_F}$, where $i \in \{N, F\}$ is used to either refer to the near-field or the far-field communication. Setting $P_r = P_t$, the transmit power at the user and DF relay that is required to achieve a capacity $\bar{R}$ is:

$$P_t = P_r = \frac{2^{\bar{R}} - 1}{\gamma'_{DF,i}}. \tag{38}$$

Therefore, the EE of full-duplex DF relaying system in near-field communication and far-field communication is given by the following Lemmas.

Lemma 11: The EE for the full-duplex relay in near-field and far-field can be expressed as

$$\eta_{DF,F,N} = \frac{B\bar{R}}{P_{D,F}} - \mathcal{F}_N(\Lambda_F, \Xi_F, P_{D,F}), \tag{39}$$

and

$$\eta_{DF,F,F} = \frac{B\bar{R}}{P_{D,F}} - \mathcal{F}_F(\Lambda_F, \Xi_F, P_{D,F}), \tag{40}$$

where $P_{D,F} = P_B + P_U + NP_F$, $\Lambda_F = \frac{2^{\bar{R}+1}-2}{\xi}$, and $\Xi_F = \frac{B\bar{R}\Lambda_F}{P_{D,F}}$.

Proof: The EE for the full-duplex relay-assisted system is obtained by replacing $P_{D,H}$ by $P_{D,F}$, Λ_D by Λ_F, and Ξ_D by Ξ_F in the expressions obtained for the half-duplex relay-assisted system. ∎

Obviously, the EE of full-duplex relay is better than the half-duplex relay because full-duplex relay can achieve the double of the rate that can deliver half-duplex relays while using the same transmit power.

V. ASYMPTOTIC RESULTS

In the following, we will derive approximations for the OP in high SNR regime to provide more insights.

A. RIS-ASSISTED SYSTEM

The incomplete Gamma function in (9) possesses the following Taylor expansion:

$$\gamma\left(\Psi_N(d_{m,1}, d_{m,2}), \frac{\sqrt{x}}{\sqrt{\bar{\gamma}}\Theta_N(d_{m,1}, d_{m,2})}\right)$$

$$= \sum_{n=0}^{\infty}\frac{(-1)^n\left(\frac{\sqrt{x}}{\sqrt{\bar{\gamma}}\Theta_N(d_{m,1}, d_{m,2})}\right)^{\Psi_N(d_{m,1}, d_{m,2})+n}}{n!\left(\Psi_N(d_{m,1}, d_{m,2}) + n\right)}.$$

Keeping the first two terms and neglecting the higher order terms in the high SNR regime, $F_{\gamma_{m,N}}^A(x|d_{m,1}, d_{m,2}.)$ can be approximated as

$$F_{\gamma_{m,N}}^A(x|d_{m,1}, d_{m,2})$$

$$\approx \frac{\left(\frac{\sqrt{x}}{\sqrt{\bar{\gamma}}\Theta_N(d_{m,1},d_{m,2})}\right)^{\Psi_N(d_{m,1},d_{m,2})}}{\Gamma\left(\Psi_N(d_{m,1},d_{m,2})\right)\Psi_N(d_{m,1},d_{m,2})}$$
$$- \frac{\left(\frac{\sqrt{x}}{\sqrt{\bar{\gamma}}\Theta_N(d_{m,1},d_{m,2})}\right)^{\Psi_N(d_{m,1},d_{m,2})+1}}{\Gamma\left(\Psi_N(d_{m,1},d_{m,2})\right)\left(\Psi_N(d_{m,1},d_{m,2})+1\right)}. \quad (41)$$

Based on the approximation $r_U \approx d_{m,2}$ and plugging (14) to (41), the CDF of $\gamma_{RIS,N}$ can be approximated as (42) shown at the bottom of the page, where $\varpi_i = \frac{R_1(\vartheta_i+1)}{2}$.

Similarly, the CDF of SNR $\gamma_{m,F}$ in the far-field can be approximated as

$$F_{\gamma_{m,F}}^A\left(x|d_{m,1},d_{m,2}\right) \approx \frac{\left(\Omega\sqrt{xd_{m,1}^{\eta_1}d_{m,2}^{\eta_2}}\right)^{\Psi_F}}{\Gamma(\Psi_F)\Psi_F}$$
$$- \frac{\left(\Omega\sqrt{xd_{m,1}^{\eta_1}d_{m,2}^{\eta_2}}\right)^{\Psi_F+1}}{\Gamma(\Psi_F)(\Psi_F+1)}. \quad (43)$$

Therefore, the asymptotic expression for $F_{\gamma_{RIS},F}^A(x)$ can be derived as

$$F_{\gamma_{RIS,F}}^A(x) \approx \exp\left\{\zeta_1 + 2\pi\int_{R_1}^{R_2} d_{m,1}\right.$$
$$\times \left.\left[\frac{\left(\Omega\sqrt{xd_{m,1}^{\eta_1}r_U^{\eta_2}}\right)^{\Psi_F}}{\Gamma(\Psi_F)\Psi_F}\frac{\left(\Omega\sqrt{xd_{m,1}^{\eta_1}r_U^{\eta_2}}\right)^{\Psi_F+1}}{\Gamma(\Psi_F)(\Psi_F+1)}\right]d\,d_{m,1}\right\}$$
$$= \exp\left\{\zeta_1 + 2\pi\left[\frac{2\left(\Omega\sqrt{xr_U^{\eta_2}}\right)^{\Psi_F}D_1}{(\eta_1\Psi_F+4)\Gamma(\Psi_F)\Psi_F}\right.\right.$$
$$\left.\left.- \frac{2\left(\Omega\sqrt{xd_{m,1}^{\eta_1}r_U^{\eta_2}}\right)^{\Psi_F+1}D_2}{(\eta_1(\Psi_F+1)+4)\Gamma(\Psi_F)(\Psi_F+1)}\right]\right\}, \quad (44)$$

where $D_1 = R_2^{\frac{\eta_1\Psi_F+4}{2}} - R_1^{\frac{\eta_1\Psi_F+4}{2}}$, and $D_2 = R_2^{\frac{\eta_1(\Psi_F+1)+4}{2}} - R_1^{\frac{\eta_1(\Psi_F+1)+4}{2}}$.

Remark 1: A careful investigation of the end-to-end SNR for near-field and far-field communication shown in (42) and (44) reveal that their distributions go to constants when $\bar{\gamma} \to \infty$, which are given by

$$F_{\gamma_{RIS,N}}^A = \exp\left\{-\pi\rho R_1^2\right\}, \quad (45)$$

and

$$F_{\gamma_{RIS,F}}^A = \exp\left\{-\pi\rho\left(R_2^2 - R_1^2\right)\right\}. \quad (46)$$

These two terms equal to the probabilities that there are no RIS candidates either in the far-field and the near-field, which means that in the high SNR, the outage occurs when there is no RIS that can be used to assist the transmission. This suggests that the outage performance can be significantly improved when RIS are densely deployed, leading to increased RIS selection diversity. We further note that since the outage probabilities do not decrease as $\bar{\gamma}$ increases, the diversity order calculated through $DO = -\lim_{\bar{\gamma}\to\infty}\frac{P_{out}(\bar{\gamma})}{\log\bar{\gamma}}$ is zero, where $P_{out}(\bar{\gamma})$ refers to $F_{\gamma_{RIS,N}}^A$ for the near-field communication and $F_{\gamma_{RIS,F}}^A$ for the far-field communication.

B. RELAY-ASSISTED SYSTEM

The exponential matrix $\exp(\frac{x}{\gamma}\mathbf{A}_1(d_{m,1}))$ in (21) can be re-presented by power series as $\exp(\frac{x}{\gamma}\mathbf{A}_1(d_{m,1})) = \sum_{k=0}^{\infty}\frac{x^k}{\gamma^k k!}\mathbf{A}_1(d_{m,1})^k$. Keeping the first two terms and neglecting the higher order terms in high SNR regime, the CDF of $\gamma_{Um,N}$ achieved by m-th relay conditioned on $d_{m,1}$ can be given by

$$F_{\gamma_{Um,N}}^A\left(x|d_{m,1}\right) \approx 1 - \mathbf{e}^T\left(\mathbf{I}_N - \frac{x}{\gamma}\mathbf{A}_1(d_{m,1})\right)\mathbf{e}_1, \quad (47)$$

The CDF of γ_{mB} can be approximated through the same way as

$$F_{\gamma_{mB}}^A(x) \approx 1 - \left(1 - r_U^{\eta_2}\frac{x}{\gamma}\right)\sum_{j=0}^{N-1}\frac{r_U^{j\eta_2}x^j}{\gamma^j j!}. \quad (48)$$

Thus, the asymptotic CDF of $\gamma_{UmB,N} = \min\{\gamma_{Um,N}, \gamma_{mB}\}$ conditioning on $d_{m,1}$ is

$$F_{\gamma_{UmB,N}}^A\left(x|d_{m,1}\right) \approx 1 - \mathbf{e}^T\left(\mathbf{I}_N - \frac{x}{\gamma}\mathbf{A}_1(d_{m,1})\right)\mathbf{e}_1$$
$$\times \left(1 - r_U^{\eta_2}\frac{x}{\gamma}\right)\sum_{j=0}^{N-1}\frac{r_U^{j\eta_2}x^j}{\gamma^j j!}, \quad (49)$$

from which we obtain the asymptotic CDF of γ_{DF} in the near-field as

$$F_{\gamma_{DF,N}}^A(x) \approx \exp\left\{-\rho\int_0^{R_1}\int_0^{2\pi} d_{m,1}\mathbf{e}^T\exp\left(\frac{x}{\gamma}\mathbf{A}(d_{m,1})\right)\mathbf{e}_1\right.$$

$$F_{\gamma_{RIS,N}}^A(x) = \exp\left\{-\pi\rho R_1^2 + 2\pi\rho\int_0^{R_1} d_{m,1}\left[\frac{\left(\frac{\sqrt{x}}{\sqrt{\bar{\gamma}}\Theta_N(d_{m,1})}\right)^{\Psi_N(d_{m,1})}}{\Gamma\left(\Psi_N(d_{m,1})\right)\Psi_N(d_{m,1})} - \frac{\left(\frac{\sqrt{x}}{\sqrt{\bar{\gamma}}\Theta_N(d_{m,1})}\right)^{\Psi_N(d_{m,1})+1}}{\Gamma\left(\Psi_N(d_{m,1})\right)\left(\Psi_N(d_{m,1})+1\right)}\right]d\,d_{m,1}\right\}$$
$$= \exp\left\{-\pi\rho R_1^2 + \pi\rho R_1\sum_{i=1}^{W_R} w_R\sqrt{1-\vartheta_i^2}\,\varpi_i\left[\frac{\left(\frac{\sqrt{x}}{\sqrt{\bar{\gamma}}\Theta_N(\varpi_i)}\right)^{\Psi_N(\varpi_i)}}{\Gamma\left(\Psi_N(\varpi_i)\right)\Psi_N(\varpi_i)} - \frac{\left(\frac{\sqrt{x}}{\sqrt{\bar{\gamma}}\Theta_N(\varpi_i)}\right)^{\Psi_N(\varpi_i)+1}}{\Gamma\left(\Psi_N(\varpi_i)\right)\left(\Psi_N(\varpi_i)+1\right)}\right]\right\} \quad (42)$$

$$\times \exp\left(-r_U^{\eta_2}\frac{x}{\bar{\gamma}}\right)\sum_{j=0}^{N-1}\frac{r_U^{j\eta_2}x^j}{\bar{\gamma}^j j!}\mathrm{d}d_{m,1}\mathrm{d}\theta\Bigg\}$$

$$\approx \exp\Bigg\{-\pi\rho R_1\sum_{i=1}^{W_D}w_D\sqrt{1-v_i^2}\left(1-r_U^{\eta_2}\frac{x}{\bar{\gamma}}\right)$$

$$\times \sum_{j=0}^{N-1}\frac{r_U^{j\eta_2}x^j}{\bar{\gamma}^j j!}\times\frac{R_1(v_i+1)}{2}\mathbf{e}^T$$

$$\times \left(\mathbf{I}_N-\frac{x}{\bar{\gamma}}\mathbf{A}_1\left(\frac{R_1(v_i+1)}{2}\right)\right)\mathbf{e}_1\Bigg\}. \tag{50}$$

Similarly, the asymptotic CDF of $\gamma_{UmB,F}=\min\{\gamma_{Um,F},\gamma_{mB}\}$ in the far-field scenario conditioning on $d_{m,1}$ is given by:

$$F_{\gamma_{UmB,F}}^A\left(x|d_{m,1}\right)\approx 1-\left(1-\frac{x}{\bar{\gamma}}d_{m,1}^{\eta_1}\right)\sum_{i=0}^{N-1}\frac{d_{m,1}^{i\eta_1}x^i}{\bar{\gamma}^i i!}$$

$$\times \left(1-r_U^{\eta_2}\frac{x}{\bar{\gamma}}\right)\sum_{j=0}^{N-1}\frac{r_U^{j\eta_2}x^j}{\bar{\gamma}^j j!}, \tag{51}$$

from which we obtain the asymptotic CDF of $\gamma_{DF,F}$ in the far-field setting as:

$$F_{\gamma_{DF,F}}^A(x)\approx \exp\Bigg\{-\rho\int_{R_1}^{R_2}\int_0^{2\pi}d_{m,1}\left(1-\frac{x}{\bar{\gamma}}d_{m,1}^{\eta_1}\right)$$

$$\times \sum_{i=0}^{N-1}\frac{d_{m,1}^{i\eta_1}x^i}{\bar{\gamma}^i i!}\left(1-\frac{x}{\bar{\gamma}}r_U^{\eta_2}\right)\sum_{j=0}^{N-1}\frac{r_U^{j\eta_2}x^j}{\bar{\gamma}^j j!}\mathrm{d}d_{m,1}\mathrm{d}\theta\Bigg\}$$

$$= \exp\Bigg\{-2\pi\rho\sum_{i=0}^{N-1}\left(\frac{D_{3,i}}{i\eta_1+2}-\frac{D_{4,i}x}{\bar{\gamma}(i\eta_1+2+\eta_1)}\right)$$

$$\times \frac{x^i}{\bar{\gamma}^i i!}\left(1-\frac{x}{\bar{\gamma}}r_U^{\eta_2}\right)\sum_{j=0}^{N-1}\frac{r_U^{j\eta_2}x^j}{\bar{\gamma}^j j!}\Bigg\}, \tag{52}$$

where $D_{3,i}=R_2^{i\eta_1+2}-R_1^{i\eta_1+2}$ and $D_{4,i}=R_2^{i\eta_1+2+\eta_1}-R_1^{i\eta_1+2+\eta_1}$.

Remark 2: Similar to the asymptotic results of RIS-assisted system, the end-to-end outage probabilities for near-field and far-field communication shown in (50) and (52) go to constants shown in (45) and (46) when $\bar{\gamma}\to\infty$, while their corresponding diversity orders are zero.

The above derived approximation results in high SNR regime have much simpler forms than the exact ones. The approximation expression does not involve the incomplete Gamma function and the exponential function, which can simplify numerical computation.

VI. EXTENSIONS AND DISCUSSIONS FOR RIS-ASSISTED SYSTEM

In this section, some selected discussions about the performance analysis of the RIS-assisted system under more practical assumptions are provided.

A. EXISTENCE OF THE DIRECT USER-BS LINK

The above performance analysis is under the assumption that the direct link between the user and BS is fully blocked. However, the existence of the direct user-BS link in some scenarios motivates us to analyze the performance of the RIS-assisted system considering the direct link between the user and BS. Accounting for the direct link between the user and the BS, the instantaneous SNR at BS can be re-expressed as:

$$\gamma_{m,N}^D=\frac{P_t\left|\sum_{n=1}^N\frac{\alpha_{m,n}}{d_{m,n,1}^{\frac{\eta_1}{2}}}\frac{\beta_{m,n}}{d_{m,2}^{\frac{\eta_2}{2}}}e^{j(\phi_{m,n}-\theta_{m,n}-\varphi_{m,n})}+\frac{\alpha_d e^{-j\theta_d}}{r_U^{\frac{\eta_d}{2}}}\right|^2}{P_L N_0}, \tag{53}$$

where α_d represents the amplitude of the direct user-BS link and is assumed to follow a Rayleigh distributed random variable, θ_d denotes the phase shift of the direct user-BS channel, and η_d is its associated path-loss exponent. Therefore, the optimal reflection coefficients can be set as $\phi_{m,n}=-\theta_d+\theta_{m,n}+\varphi_{m,n}$. Under the use of optimal phases, the SNR associated with communication through the m-th RIS is:

$$\gamma_{m,N}^D=\frac{P_t\left|\sum_{n=1}^N\frac{\alpha_{m,n}}{d_{m,n,1}^{\frac{\eta_1}{2}}}\frac{\beta_{m,n}}{d_{m,2}^{\frac{\eta_2}{2}}}+\frac{\alpha_d}{r_U^{\frac{\eta_d}{2}}}\right|^2}{P_L N_0}. \tag{54}$$

The expectation and variance of $\sum_{n=1}^N\frac{\alpha_{m,n}}{d_{m,n,1}^{\frac{\eta_1}{2}}}\frac{\beta_{m,n}}{d_{m,2}^{\frac{\eta_2}{2}}}+\frac{\alpha_d e^{-j\theta_d}}{r_U^{\frac{\eta_d}{2}}}$ conditioned $d_{m,n,1}$, $d_{m,2}$ and α_d can be obtained as

$$\mathbb{E}\left[\sum_{n=1}^N\frac{\alpha_{m,n}}{d_{m,n,1}^{\frac{\eta_1}{2}}}\frac{\beta_{m,n}}{d_{m,2}^{\frac{\eta_2}{2}}}+\frac{\alpha_d}{r_U^{\frac{\eta_d}{2}}}|d_{m,n,1},d_{m,2},\alpha_d\right]$$

$$=\sum_{n=1}^N\frac{\pi}{4d_{m,n,1}^{\frac{\eta_1}{2}}d_{m,2}^{\frac{\eta_2}{2}}}+\frac{\alpha_d}{r_U^{\frac{\eta_d}{2}}}, \tag{55}$$

and

$$\mathrm{var}\left[\sum_{n=1}^N\frac{\alpha_{m,n}}{d_{m,n,1}^{\frac{\eta_1}{2}}}\frac{\beta_{m,n}}{d_{m,2}^{\frac{\eta_2}{2}}}+\frac{\alpha_d}{r_U^{\frac{\eta_d}{2}}}|d_{m,n,1},d_{m,2},\alpha_d\right]$$

$$=\sum_{n=1}^N\frac{1-\frac{\pi^2}{16}}{d_{m,n,1}^{\eta_1}d_{m,2}^{\eta_2}}. \tag{56}$$

Therefore, the $\sum_{n=1}^N\frac{\alpha_{m,n}}{d_{m,n,1}^{\frac{\eta_1}{2}}}\frac{\beta_{m,n}}{d_{m,2}^{\frac{\eta_2}{2}}}+\frac{\alpha_d}{r_U^{\frac{\eta_d}{2}}}$ can be approximated through the Gamma distribution with shape parameter

$$\Psi_N^D(d_{m,1},d_{m,2},\alpha_d)=\frac{\left(\sum_{n=1}^N\frac{\pi}{4d_{m,n,1}^{\frac{\eta_1}{2}}d_{m,2}^{\frac{\eta_2}{2}}}+\frac{\alpha_d}{r_U^{\frac{\eta_d}{2}}}\right)^2}{\sum_{n=1}^N\frac{1-\frac{\pi^2}{16}}{d_{m,n,1}^{\eta_1}d_{m,2}^{\eta_2}}}$$

and scale parameter

$$\Theta_N^D\left(d_{m,1}, d_{m,2}, \alpha_d\right) = \frac{\sum_{n=1}^N \frac{1-\frac{\pi^2}{16}}{d_{m,n,1}^{\eta_1} d_{m,2}^{\eta_2}}}{\sum_{n=1}^N \frac{\pi}{4d_{m,n,1}^{\frac{\eta_1}{2}} d_{m,2}^{\frac{\eta_2}{2}}} + \frac{\alpha_d}{r_U^{\frac{\eta_d}{2}}}}.$$

Similar to (9), the CDF of $\gamma_{m,N}^D$ conditioned on $d_{m,1}$, $d_{m,2}$, and α_d can be approximated as

$$F_{\gamma_{m,N}^D}\left(x \middle| d_{m,1}, d_{m,2}, \alpha_d\right) = \frac{1}{\Gamma\left(\Psi_N^D\left(d_{m,1}, d_{m,2}, \alpha_d\right)\right)}$$
$$\times \gamma\left(\Psi_N^D\left(d_{m,1}, d_{m,2}, \alpha_d\right), \frac{\sqrt{x}}{\sqrt{\bar{\gamma}}\Theta_N^D\left(d_{m,1}, d_{m,2}, \alpha_d\right)}\right). \tag{57}$$

Therefore, the CDF of $\gamma_{RIS,N}^D$ based on the approximation $r_U \approx d_{m,2}$ can be calculated as

$$F_{\gamma_{RIS,N}^D}(x) = \int_0^\infty \exp\left\{-\pi\rho R_1^2 + 2\pi\rho\int_0^{R_1} \frac{d_{m,1}}{\Gamma\left(\Psi_N^D\left(d_{m,1}, \alpha_d\right)\right)}\right.$$
$$\times \left. \gamma\left(\Psi_N^D\left(d_{m,1}, \alpha_d\right), \frac{x}{\bar{\gamma}\Theta_N^D\left(d_{m,1}, \alpha_d\right)}\right) dd_{m,1}\right\}$$
$$\times 2\alpha_d \exp\left\{-\alpha_d^2\right\} d\alpha_d. \tag{58}$$

Similarly, the instantaneous SNR of the RIS-assisted system with direct user-BS link in the far-field communication with optimal phase shifts is given by

$$\gamma_{m,F}^D = \frac{P_t \left| \frac{\sum_{n=1}^N \alpha_{m,n}\beta_{m,n}}{d_{m,1}^{\frac{\eta_1}{2}} d_{m,2}^{\frac{\eta_2}{2}}} + \frac{\alpha_d}{r_U^{\frac{\eta_d}{2}}} \right|^2}{P_L N_0}. \tag{59}$$

We also approximate $\frac{\sum_{n=1}^N \alpha_{m,n}\beta_{m,n}}{d_{m,1}^{\frac{\eta_1}{2}} d_{m,2}^{\frac{\eta_2}{2}}} + \frac{\alpha_d}{r_U^{\frac{\eta_d}{2}}}$ by the Gamma distribution with the shape parameter $\Psi_F^D = \frac{\left(\frac{N\pi}{4d_{m,1}^{\frac{\eta_1}{2}} d_{m,2}^{\frac{\eta_2}{2}}} + \frac{\alpha_d}{r_U^{\frac{\eta_d}{2}}}\right)^2}{\frac{N\left(1-\frac{\pi^2}{16}\right)}{d_{m,1}^{\eta_1} d_{m,2}^{\eta_2}}}$

and the scale parameter $\Theta_F^D = \frac{\frac{N\left(1-\frac{\pi^2}{16}\right)}{d_{m,1}^{\eta_1} d_{m,2}^{\eta_2}}}{\frac{N\pi}{4d_{m,1}^{\frac{\eta_1}{2}} d_{m,2}^{\frac{\eta_2}{2}}} + \frac{\alpha_d}{r_U^{\frac{\eta_d}{2}}}}$ using a moment

matching method. Therefore, the CDF for $\gamma_{m,F}^D$ conditioning on $d_{m,1}$, $d_{m,2}$ and α_d and the end-to-end SNR $\gamma_{RIS,F}^D$ can be obtained by replacing $\Psi_N^D(d_{m,1}, d_{m,2}, \alpha_d)$ and $\Theta_N^D(d_{m,1}, d_{m,2}, \alpha_d)$ in (57) and (58) by Ψ_F^D and Θ_F^D. Similarly, the EE in near-field and far-field can be calculated through the same way shown in Section III-B.

One can observe that the performance analysis of RIS-assisted with the direct user-BS link is much complex than the one without the direct user-BS link. Actually, it is reasonable to ignore the direct user-BS link because RIS provides much higher SNR gain than the SISO direct link, especially when using massive reflecting elements and under high deployment density.

B. MORE COMPLEX CHANNEL MODELS

Our analysis, relying on Gamma approximation, is valid also for more complex channel models including Nakagami-m fading and Rician fading. Indeed, even when other distributions are considered, the sum of the product of channel amplitudes involved in the SNR expression can be approximated by a Gamma distribution using the moment matching method. The single difference with the Rayleigh fading channels is that the computation of the moments will involve the parameters of the considered distributions. For example, assume that $\alpha_{n,m}$ is drawn from a Nakagami-m distribution with average value Ω_α and Nakagami-m fading parameter m_α, and $\beta_{n,m}$ follows a Nakagami-m distribution with average value Ω_β and Nakagami fading parameter m_β, the expectation and variance of the quantity $S_N = \sum_{n=1}^N \frac{\alpha_{m,n}\beta_{m,n}}{d_{m,n,1}^{\frac{\eta_1}{2}} d_{m,2}^{\frac{\eta_2}{2}}}$ conditioned $d_{m,n,1}$ and $d_{m,2}$ can be obtained as

$$\mathbb{E}\left[S_N \middle| d_{m,n,1}, d_{m,2}\right] = \sum_{n=1}^N \frac{E_\alpha E_\beta}{d_{m,n,1}^{\frac{\eta_1}{2}} d_{m,2}^{\frac{\eta_2}{2}}}, \tag{60}$$

and

$$\text{var}\left[S_N \middle| d_{m,n,1}, d_{m,2}\right] = \sum_{n=1}^N \frac{\left(V_\alpha + E_\alpha^2\right)\left(V_\beta + E_\beta^2\right) - E_\alpha^2 E_\beta^2}{d_{m,n,1}^{\eta_1} d_{m,2}^{\eta_2}}, \tag{61}$$

where

$$E_\alpha = \frac{\Gamma\left(m_\alpha + \frac{1}{2}\right)}{\Gamma(m_\alpha)}\left(\frac{\Omega_\alpha}{m_\alpha}\right)^{\frac{1}{2}}, \tag{62}$$

$$E_\beta = \frac{\Gamma\left(m_\beta + \frac{1}{2}\right)}{\Gamma(m_\beta)}\left(\frac{\Omega_\beta}{m_\beta}\right)^{\frac{1}{2}}, \tag{63}$$

$$V_\alpha = \Omega_\alpha\left(1 - \frac{1}{m_\alpha}\left(\frac{\Gamma\left(m_\alpha + \frac{1}{2}\right)}{\Gamma(m_\alpha)}\right)^2\right), \text{ and} \tag{64}$$

$$V_\beta = \Omega_\beta\left(1 - \frac{1}{m_\beta}\left(\frac{\Gamma\left(m_\beta + \frac{1}{2}\right)}{\Gamma(m_\beta)}\right)^2\right). \tag{65}$$

Then, S_N can be approximated through the Gamma distribution with shape parameter and scale parameter obtained by matching the expectation of S_N and its variance to those of a Gamma random variable. Based on this Gamma approximation, the performance analysis can be performed in the same way by replacing the parameters of the Gamma distribution by those obtained under the desired channel models.

VII. NUMERICAL RESULTS

In this section, we compare the OP and EE of the RIS assisted system, the half-duplex relaying system, and the full-duplex relaying system based on both simulations and analytical results. It should be noted that the OP for the
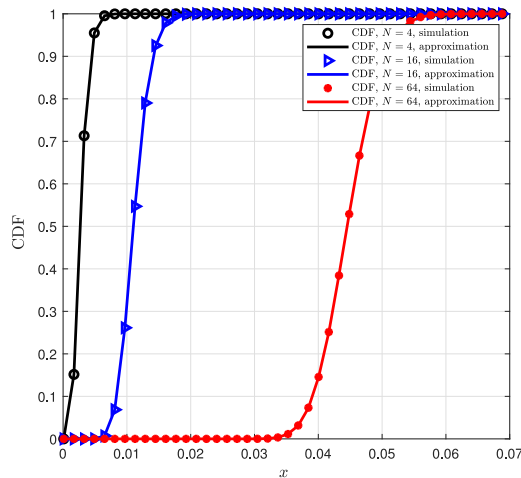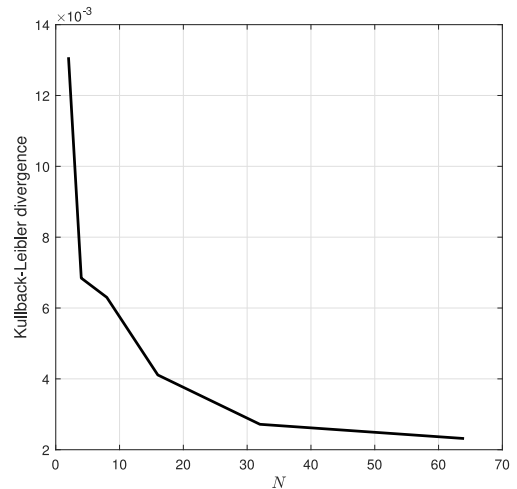
FIGURE 2. CDF of S_N in the near-field.

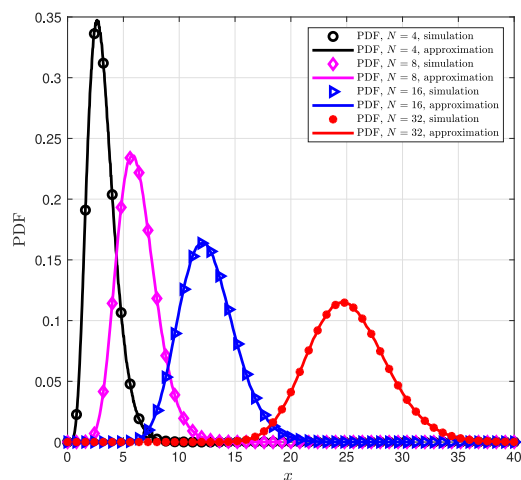**FIGURE 4.** Kullback-Leibler divergence versus *N*.
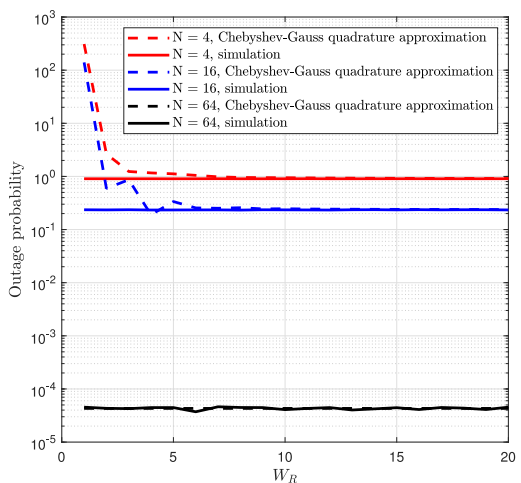

FIGURE 3. PDF of S_F in the far-field.

FIGURE 5. OP versus W_R in the near-field with $\rho = 0.05$.

full-duplex relaying system is equal to the one for the half-duplex relaying system. Hence, both relaying systems will be referred to as 'DF' in the figures representing the OP. In the figures regarding EE, the half-duplex DF relaying system is denoted by 'HD-DF', while the full-duplex DF relaying system is denoted by 'FD-DF'. Following the parameters adopted in [27], [30], [40], unless otherwise mentioned, the main parameters in our simulations are set as follows: $N_0 = -124$ dBW, $\gamma_{th} = 1$ dB, $R_1 = 8$ m, $R_2 = \sqrt{2}R_1$ m, $r_U = 150$ m, $\xi = 0.5$, $P_B = P_U = 100$ mW, $P_b = 5$ mW, $P_H = 10$ mW, $P_F = 20$ mW, $\eta_1 = \eta_2 = \eta_d = 2$, $f = 3$ GHz and $L = \frac{\lambda}{4}$.

Prior to carrying out the system performance comparison, we shall first check the accuracy of the Gamma approximation provided in **Lemma 1** and **Lemma 2**. For that, we plot in Fig. 2 the empirical CDF of S_N in the case of near-field communication along with the Gamma approximation presented in (6) for different numbers of reflecting elements. One can see from this figure that the exact CDF matches the Gamma distribution in (6), which validates the proposed

approximation. Similarly, in Fig. 3, we represent the empirical PDF of S_F along with its approximation given in (11) in the case of far-field communication. Again, we note the perfect match between both density functions, which supports the validity of the Gamma approximation. To quantify the accuracy of this approximation, we invoke the Kullback-Leibler divergence, defined as $\mathcal{D}_{KL} = E[\log \frac{f_{Ext}(x)}{f_{App}(x)}]$, where $f_{Ext}(x)$ denotes the exact PDF and $f_{App}(x)$ represents the PDF approximation. We plot in Fig. 4 the Kullback-Leibler divergence metric as a function of the number of reflecting elements N for the far-field communication. In this case $f_{App}(x)$ denotes the Gamma approximation in (11) while $f_{Ext}(x)$ is the empirical PDF of the exact distribution. As can be noted, the value of the Kullback-Leibler divergence is smaller than 10^{-3} which again supports the accuracy of the Gamma approximation. Moreover, this accuracy becomes better as the number of reflecting elements N increases, which confirms the usefulness of the Gamma approximation, especially for large reflecting surfaces.

The derived expressions are also based on the Chebyshev-Gauss quadrature approximation, which we shall verify the
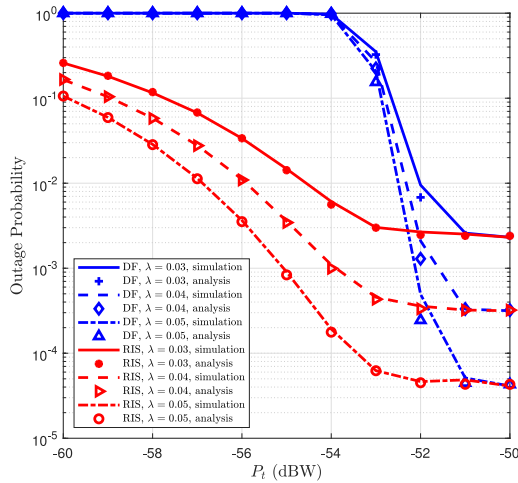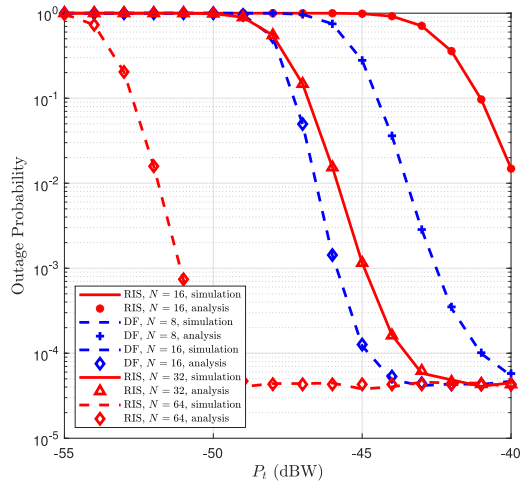
FIGURE 6. OP versus P_t in the near-field with $N = 64$.

FIGURE 7. OP versus P_t in the far-field with $\rho = 0.05$.

accuracy. Considering the near-field communication, we plot in Fig. 5 the OP of RIS assisted systems as derived in **Lemma 3** versus the Chebyshev-Gauss parameter W_R. As can be shown, the accuracy of the Chebyshev-Gauss quadrature approximation becomes even better as the number of reflecting elements increases. It also improves with W_R, going to the exact value as W_R increases. Moreover, from this experiment, it appears that a tight approximation is obtained for as much as 20 elements in the sum involved in the Chebyshev-Gauss quadrature approximation. Based on that, in all forthcoming simulations, we set the Chebyshev-Gauss parameter to 20.

A. OUTAGE PROBABILITY

Then, we conduct several experiments to compare the outage performance of the RIS-assisted system and the one of the relay-assisted system. In a first experiment, we compare the OP of the RIS-assisted system with that of DF relaying under the near-field scenario. Note that as perfect-inter-relay interference is considered, both full-duplex and half-duplex relaying system correspond to the same OP. As can be seen in Fig. 6, the RIS-assisted system shows better performance than that of the DF relaying system in the low SNR regime and goes to the same OP as the DF relaying system in the high SNR regime. The degradation in performance of the DF relaying system in the low SNR regime is because the transmit power at the relay is not sufficient to compensate for the path-loss in the second hop transmission. Moreover, it is noted that OP can be improved by increasing the deployment density ρ, leading to more RISs/relays candidates from which the best one is selected.

In the second experiment, we compare the OP of the RIS-assisted system with that of DF relaying in the far-field scenario. As shown in Fig. 7, DF relaying outperforms RIS with the same number of transmit antennas, which is opposite to the near-field. Indeed, the DF relaying system with $N = 16$ transmit antennas achieves $5 - 6$ dB gain in transmit power compared to RIS. This can be explained by

the fact that the SNR of the first hop achieved by the RIS-assisted system is low in the far-field scenario due to a higher path loss. However, the relay-assisted system is not affected by this higher path-loss since contrary to the RIS assisted system, the SNR in the second hop is independent of the path loss in the first hop due to the processing carried out at the relay, which consists in re-encoding, and retransmitting the message with the same power used to transmit it [43]. However, the performance gap can be mitigated by increasing the number of reflecting elements at RIS. About a 6 dB power gain can be reaped by adding 16 reflecting elements. As a matter of fact, compared to the DF relaying system when $N = 8$, the RIS-assisted system achieves much better performance in the low SNR regime when $N = 32$ and $N = 64$. This shows that to reduce power consumption while achieving the same or better performance, increasing the number of reflecting elements at RIS is a promising strategy. Finally, it can be noted that the OP for both near-field and far-field saturates in the high SNR regime. This behavior stems from the fact that there is a non-vanishing probability that none RIS or relays are surrounding the user to assist communication.

In the third experiment, we plot the asymptotic OP derived in Section V. As depicted in Fig. 8, the asymptotic OP matches the empirical ones in the high SNR regime. One can also observe a saturation of the OP lines in the high SNR region. The reason for such a behavior lies in that the OP is mainly related to how many RIS/relays are deployed. Since RISs and relays are distributed with the same density, the asymptotic behavior of the OP for both RISs and relays is exactly the same. This phenomenon was predicted by the high SNR asymptotic analysis (see **Remark 1** and **Remark 2**). As can also be seen, when using RISs, the OP in the far-field communication becomes better in the high SNR regime than that in the near-field communication. The reason for that is that the far-field communication is associated with area $R_2^2 - R_1^2$, which is higher than that of the near-field communication (R_1^2) when $R_2 > R_1$. As a result,
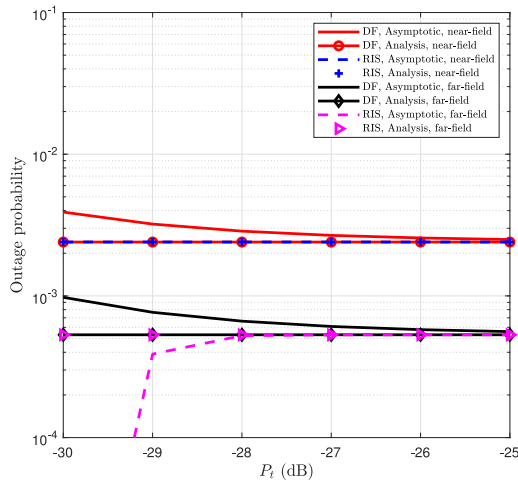
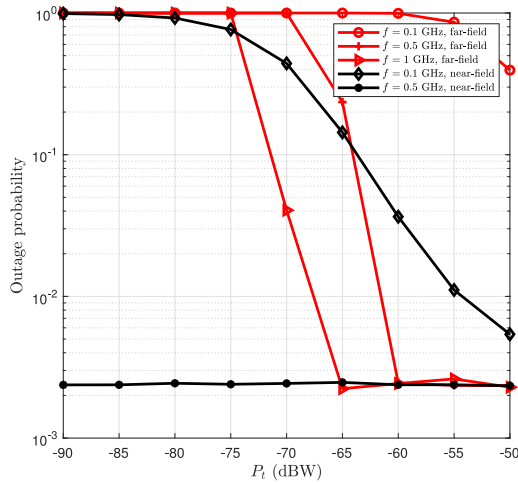**FIGURE 8.** Asymptotic OP versus P_t with $\rho = 0.03$, $N = 16$, $R_2 = 12$ m.

FIGURE 9. OP versus P_t with $\rho = 0.03$.

FIGURE 10. OP versus P_t with $\rho = 0.05$ and $N = 36$.

with more RISs present, the far-field communication benefits from a higher selection diversity, and hence presents better performance in the high SNR regime.

In Fig. 9, we investigate the impact of the carrier frequency. As can be seen from (1) and (10), on the one hand, a high carrier frequency has a negative impact on the received SNR. On the other hand, as the carrier frequency increases, the RIS size decreases. As a result, for a fixed total area for the RIS, it is possible to pack more elements when operating at a high frequency than when operating at a low frequency. Consequently, the RIS operating at a high frequency is expected to provide more diversity gain. The question is whether this diversity gain enabled by the possibility of using more elements would allow for compensating the severe path loss attenuation experienced by radio high frequency waves. To answer this question, we have performed some experiments under different carrier frequencies assuming RISs have the same size S. Assuming that the area of each element is $L^2 = (\frac{\lambda}{4})^2$, the number of elements that can be packed in a surface of size S is $N = \lfloor \frac{S}{L^2} \rfloor$. We represent in Fig. 9 the OP under a fixed total RIS size ($S = 1m^2$) for different operating frequencies. As
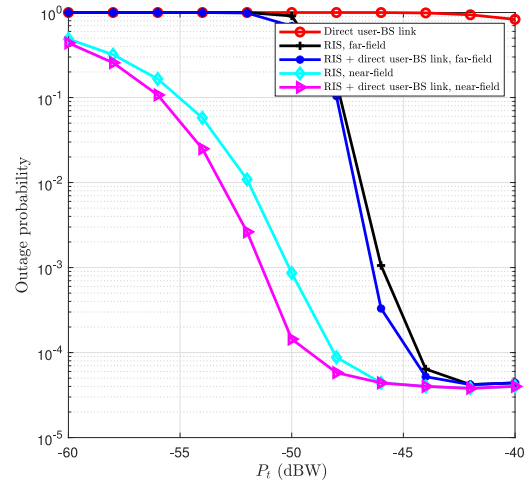
can be seen, operating over high frequencies improves the performances of both near-field and far-field communications, providing the evidence that the diversity gain offered by high frequencies enables to compensate the incurred high loss attenuation. Moreover, one can see that the outage performance in near-field communication is better than the one in far-field communication. This can be explained by the fact that near-field communication undergoes shorter distances between the transmitter and the receiver than far-field communication.

Lastly, we compare the OP achieved by the RIS-assisted system with the direct user-BS link and the one achieved by RIS-assisted without the direct user-BS link. As shown in Fig. 10, the OP of the direct user-BS link without RIS is much higher than the one of the RIS-assisted system without the direct user-BS link. Moreover, there is a small gap between the OP lines for the RIS-assisted system with the direct user-BS link and the RIS-assisted system without the direct user-BS link. This suggests that the direct link does not bring an important improvement, and as a consequence the direct SISO user-BS link can be reasonably ignored to simplify performance analysis while keeping the same performance trends. Particularly, one can see that the OP achieved in the near-field communication is lower than the OP achieved in the far-field communication, which is the same as the results obtained in Fig. 9. This again confirms the possibility of ignoring the direct user-BS link for SISO RIS assisted systems even in near field communication.

B. ENERGY EFFICIENCY

In this subsection, we analyze the behavior of EE versus a fixed achievable rate $\overline{R}$. As can be seen in Fig. 11, the half-duplex DF relaying becomes the worst choice, while the RIS is the best option in the near-field. We can also note that the path loss factor in the second hop plays an important role in system performance, with EEs associated with the three technologies with $\eta_2 = 2.5$ being almost half of those with $\eta_2 = 2$. It also can be seen that RIS counteract better
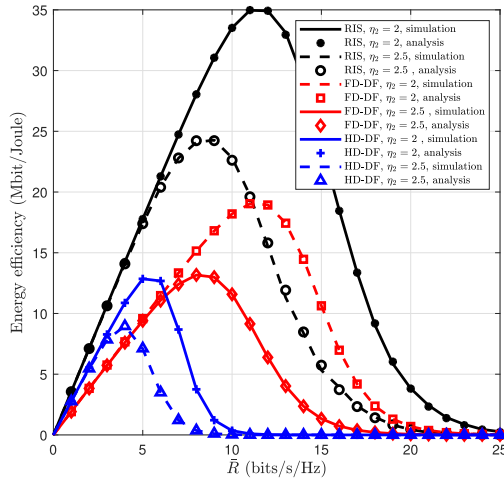
FIGURE 11. EE versus $\bar{R}$ in near-field with $\rho = 0.03$ and $N = 16$.
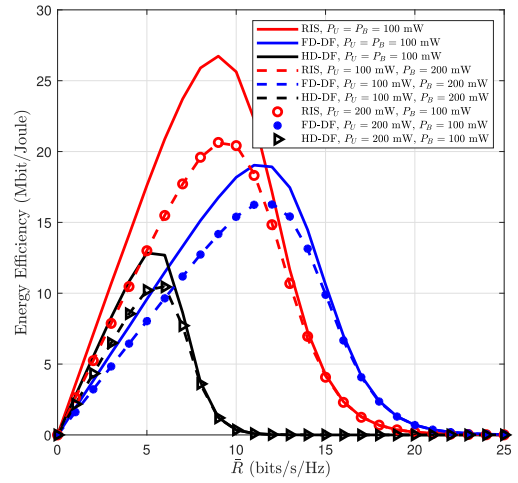
FIGURE 13. EE versus $\bar{R}$ in far-field with $\rho = 0.03$ and $N = 16$.
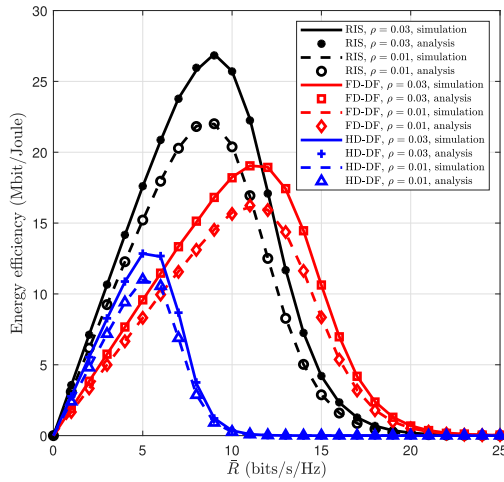
FIGURE 12. EE versus $\bar{R}$ in far-field with $N = 16$.
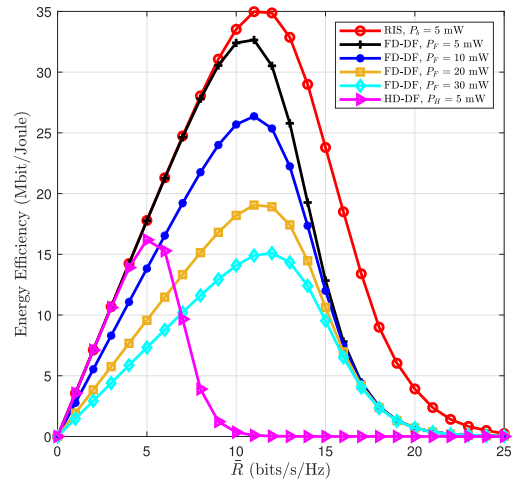
FIGURE 14. EE versus $\bar{R}$ in near-field with $\rho = 0.03$ and $N = 16$.

the effect of the path-loss: RISs experiencing higher path loss provides much better performance than half-duplex DF relaying with lower path loss.

On the other hand, in the far-field case, as illustrated in Fig. 12 it is the full-duplex relaying that becomes the best choice in the high data rate regime, while RIS is still the best option in the low data rate regime. However, over the whole range of required achievable rates, the maximum EE achieved by RIS is higher than the one achieved by full-duplex relaying. Moreover, it can be noted that increasing the deployment density of RISs/relays plays a positive role in EE, with a higher improvement in the performance for the RIS-assisted system than for the relay-assisted system. As a conclusion, it clearly appears that the RIS-assisted system is the most energy-efficient solution with the same number of receiving and transmitting antennas as relays. The system performance can be greatly improved when RISs are sufficiently densely deployed. Moreover, compared to the far-field case, all technologies achieve higher EE in the near-field scenario because signals experience more serious path

loss in far-field communication with the same deployment area.

To investigate the impact of the hardware dissipated power, we plot in Fig. 13 the EE with respect to $\bar{R}$ for various combinations of P_B and P_U. It can be easily understood that these powers have a negative impact on the EE as they correspond to inevitable powers dissipated by the hardware. As can be easily predicted from theoretical expressions for EE, the EE curve with $P_B = 200$ mW and $P_U = 100$ mW overlaps with that with $P_B = 100$ mW and $P_U = 200$ mW, which shows that the hardware dissipated power consumption at the user and the base station have the same impact.

The good performance of RIS assisted systems in terms of EE compared to relay assisted systems can be explained as follows: 1) The RIS is composed of passive elements that dissipate little power (P_b) as compared to that of the full-duplex DF relay (P_F) and the half-duplex DF relay systems (P_H) 2) It directly reflects the impinging signal and does not require any transmission power contrary to the relay assisted system. Both of these factors contribute to the RIS outperforming relay assisted systems. In all previous experiments, the values
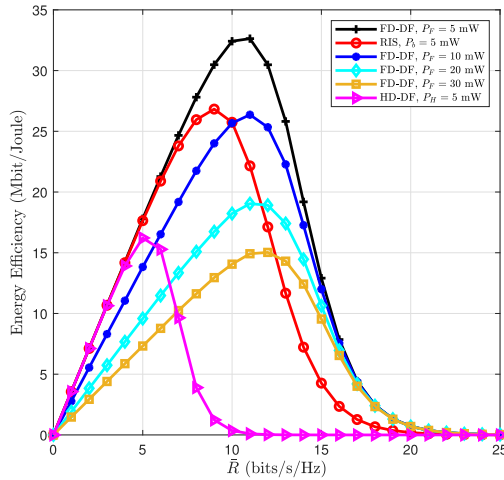
FIGURE 15. EE versus $\bar{R}$ in far-field with $\rho = 0.03$ and $N = 16$.

of P_F, P_H, and P_b are chosen such that $P_F > P_H > P_b$, since full-duplex relays require more power than half-duplex relays to mitigate self-interference, and RISs are composed of passive elements that dissipate little power. However, to further understand the role of P_b in the performance of RIS assisted systems, we set it in Figs. 14-15 such that $P_H = P_F = P_b$. Such an assumption is unrealistic, but it allows us to see whether in this case the RIS can still bring an improvement in terms of EE by only dispensing with the transmission power used at relays. As shown in Fig. 14, the RIS-assisted system still outperforms the half-duplex DF relaying system and full-duplex DF relaying system in near-field communication when $P_H = P_F = P_b = 5$ mW. Different from the near-field communication, the full-duplex DF relaying becomes the best choice in far-field communication with $P_b = P_H = P_F$, as given in Fig. 15. It indicates that the full-duplex relay requires the lowest total transmit power to achieve the same target rate. Investigating the impact of P_F on EE, we can see that the EE for the full-duplex DF relaying system decreases as P_F increases. It becomes lower than that of the half-duplex relaying system and the RIS-assisted system (with $P_H = 5$ mW and $P_b = 5$ mW)in the low data rate regime, which agrees with the results in Fig. 12. The maximum value of the EE achieved by the full-duplex DF relaying system is even smaller than the one of the half-duplex DF relaying system when P_F is set to 30 mW. Furthermore, the half-duplex relay is always the worst choice compared to the other two technologies in the high data rate regime for both near-field and far-field communication.

Finally, we note that as can be seen from these figures, there is a perfect match between the theoretical results and those obtained by numerical simulations.

VIII. CONCLUSION

This work is among the first studies to make a fair comparison between spatially-distributed RISs and relay-assisted systems in both near-field and far-field communication scenarios. Both technologies have the common goal of forwarding the received signal to the destination with the

difference that, unlike relays, RISs are composed of passive elements that consume little amounts of power. As a major outcome, we prove that RISs achieve the best performance in terms of EE, especially when deployed near the transmitter. Moreover, RISs allows for improved system performance in terms of OP and EE when equipped with more reflecting elements or densely deployed. In conclusion, it clearly appears that the use of RIS is a promising technology that allows for a better EE than relay-assisted systems.

APPENDIX A
PROOF OF LEMMA 1

Since $\alpha_{m,n}$ and $\beta_{m,n}$ are independent Rayleigh distributed random variables, the mean value of their product is

$$\mathbb{E}\left[\frac{\alpha_{m,n}}{d_{m,n,1}^{\frac{\eta_1}{2}}}\frac{\beta_{m,n}}{d_{m,2}^{\frac{\eta_2}{2}}}\Big|d_{m,n,1}, d_{m,2}\right] = \frac{\pi}{4d_{m,n,1}^{\frac{\eta_1}{2}}d_{m,2}^{\frac{\eta_2}{2}}}, \quad (66)$$

while the variance is

$$\mathrm{var}\left[\frac{\alpha_{m,n}}{d_{m,n,1}^{\frac{\eta_1}{2}}}\frac{\beta_{m,n}}{d_{m,2}^{\frac{\eta_2}{2}}}\Big|d_{m,n,1}, d_{m,2}\right] = \frac{1 - \frac{\pi^2}{16}}{d_{m,n,1}^{\eta_1}d_{m,2}^{\eta_2}}. \quad (67)$$

We can obtain the expectation and variance of S_N as

$$\mathbb{E}\left[S_N\big|d_{m,n,1}, d_{m,2}\right] = \sum_{n=1}^{N}\frac{\pi}{4d_{m,n,1}^{\frac{\eta_1}{2}}d_{m,2}^{\frac{\eta_2}{2}}}, \quad (68)$$

$$\mathrm{var}\left[S_N\big|d_{m,n,1}, d_{m,2}\right] = \sum_{n=1}^{N}\frac{1 - \frac{\pi^2}{16}}{d_{m,n,1}^{\eta_1}d_{m,2}^{\eta_2}}. \quad (69)$$

For Gamma distribution $\Gamma(\Psi_N, \Theta_N)$ with shape parameter Ψ_N and scale parameter Θ_N, its expectation and variance are $\Psi_N\Theta_N$ and $\Psi_N\Theta_N^2$. Thus, we can obtain Ψ_N and Θ_N through $\Psi_N\Theta_N = \sum_{n=1}^{N}\frac{\pi}{4d_{m,n,1}^{\frac{\eta_1}{2}}d_{m,2}^{\frac{\eta_2}{2}}}$ and $\Psi_N\Theta_N^2 = \sum_{n=1}^{N}\frac{1-\frac{\pi^2}{16}}{d_{m,n,1}^{\eta_1}d_{m,n,2}^{\eta_2}}$, from which we can easily deduce

$$\Psi_N(d_{m,1}, d_{m,2}) = \frac{\left(\sum_{n=1}^{N}\frac{\pi}{4d_{m,n,1}^{\frac{\eta_1}{2}}d_{m,2}^{\frac{\eta_2}{2}}}\right)^2}{\sum_{n=1}^{N}\frac{1-\frac{\pi^2}{16}}{d_{m,n,1}^{\eta_1}d_{m,2}^{\eta_2}}} \quad \text{and} \quad (70)$$

$$\Theta_N(d_{m,1}, d_{m,2}) = \frac{\sum_{n=1}^{N}\frac{1-\frac{\pi^2}{16}}{d_{m,n,1}^{\eta_1}d_{m,2}^{\eta_2}}}{\sum_{n=1}^{N}\frac{\pi}{4d_{m,n,1}^{\frac{\eta_1}{2}}d_{m,2}^{\frac{\eta_2}{2}}}}. \quad (71)$$

Therefore, based on the Gamma distribution $\Gamma(\Psi_N(d_{m,1}, d_{m,2}), \Theta_N(d_{m,1}, d_{m,2}))$, the PDF and CDF of S_N conditioned on $d_{m,1}$ and $d_{m,2}$ can be obtained in (5) and (6). This completes the proof of **Lemma 1**.

APPENDIX B
PROOF OF LEMMA 3

Based on the approximation $r_U \approx d_{m,2}$ and applying (14) to (9), the CDF of $\gamma_{RIS,N}$ can be calculated as

$$
F_{\gamma_{RIS,N}}(x) = \exp\left\{-\rho \int_0^{R_1} \int_0^{2\pi} d_{m,1} \left[1 - \frac{1}{\Gamma\big(\Psi_N(d_{m,1})\big)}\right.\right.
$$
$$
\times \gamma\left(\Psi_N(d_{m,1}), \frac{x}{\bar{\gamma}\,\Theta_N(d_{m,1})}\right)\bigg]
$$
$$
\times \mathrm{d}d_{m,1}\mathrm{d}\omega\bigg\}
$$
$$
= \exp\left\{-\pi\rho R_1^2 + 2\pi\rho \int_0^{R_1} \frac{d_{m,1}}{\Gamma\big(\Psi_N(d_{m,1})\big)}\right.
$$
$$
\left.\times \gamma\left(\Psi_N(d_{m,1}), \frac{x}{\bar{\gamma}\,\Theta_N(d_{m,1})}\right)\mathrm{d}d_{m,1}\right\}. \tag{72}
$$

In the near-field communication, the expressions of $\Psi_N(d_{m,1})$ and $\Theta_N(d_{m,1})$ are complex, making the simplification of the above integral rather hard. As a solution, we invoke the Chebyshev-Gauss quadrature approximation, which is presented as: $\int_{-1}^1 \frac{f(x)}{\sqrt{1-x^2}}dx \approx \sum_{i=1}^W wf(x_i)$ with $x_i = \cos(\frac{2i-1}{2W}\pi)$ and the weight $w = \frac{\pi}{W}$. Therefore, through variable substitution, the integration can be re-expressed as

$$
F_{\gamma_{RIS,N}}(x)
$$
$$
= \exp\left\{-\pi\rho R_1^2 + \pi\rho R_1 \int_{-1}^1 \frac{\frac{R_1(y+1)}{2}}{\Gamma\left(\Psi_N\left(\frac{R_1(y+1)}{2}\right)\right)}\right.
$$
$$
\left.\times \gamma\left(\Psi_N\left(\frac{R_1(y+1)}{2}\right), \frac{x}{\bar{\gamma}\,\Theta_N\left(\frac{R_1(y+1)}{2}\right)}\right)\mathrm{d}y\right\}. \tag{73}
$$

Thus, the CDF of $\gamma_{RIS,N}$ can be finally calculated as (15) through the Chebyshev-Gauss quadrature approximation. This completes the proof of **Lemma 3**.

APPENDIX C
PROOF OF LEMMA 5

Defining $\gamma'_{RIS,N} = \max_{m\in\mathcal{S}}\left\{\frac{\left(\sum_{n=1}^N \frac{\alpha_{m,n}}{\eta_1} \frac{\beta_{m,n}}{\eta_2}\right)^2}{\frac{d_{m,n,1}^2}{2} \frac{d_{m,2}^2}{2}}{P_L N_0}\right\}$, the necessary transmit power P_t in near-field to achieve a fixed channel capacity $\bar{R}$ as:

$$
P_t = \frac{2^{\bar{R}} - 1}{\mathbb{E}\big[\gamma'_{RIS,N}\big]}. \tag{74}
$$

Plugging (74) into η, the EE for a RIS-assisted system can be expressed as:

$$
\eta_{RIS,N} = \mathbb{E}\left[\frac{B\bar{R}}{\frac{2^{\bar{R}}-1}{\xi\gamma'_{RIS,N}} + P_B + NP_b + P_U}\right]
$$

$$
= \mathbb{E}\left[\frac{B\bar{R}\gamma'_{RIS,N}}{\frac{2^{\bar{R}}-1}{\xi} + (P_B + NP_b + P_U)\gamma'_{RIS,N}}\right]
$$
$$
= \mathbb{E}\left[\frac{B\bar{R}}{P_R} - \frac{\Xi_R}{\Lambda_R + P_R\gamma'_{RIS,N}}\right]
$$
$$
= \frac{B\bar{R}}{P_R} - \Xi_R \mathbb{E}\left[\frac{1}{\Lambda_R + P_R\gamma'_{RIS,N}}\right], \tag{75}
$$

where $P_R = P_B + NP_b + P_U$, $\Lambda_R = \frac{2^{\bar{R}}-1}{\xi}$ and $\Xi_R = \frac{B\bar{R}\Lambda_R}{P_R}$. Using the relation $\mathbb{E}_X(x) = \int_0^\infty \Pr\{X > t\}dt$ which holds for X positive random variable, we have

$$
\mathbb{E}\left[\frac{1}{\Lambda_R + P_R\gamma'_{RIS,N}}\right] = \int_0^\infty \Pr\left\{\frac{1}{\Lambda_R + P_R\gamma'_{RIS}} > t\right\}dt
$$
$$
= \int_0^{\frac{1}{\Lambda_R}} \Pr\left\{\gamma'_{RIS,N} < \frac{1}{tP_R} - \frac{\Lambda_R}{P_R}\right\}dt
$$
$$
\approx \int_0^{\frac{1}{\Lambda_R}} \exp\left\{-\pi\rho R_1^2 + 2\pi\rho \sum_{i=1}^{W_R} w_R\sqrt{1 - \vartheta_i^2}\right.
$$
$$
\left.\times \frac{\frac{R_1(\vartheta_i+1)}{2}}{\Gamma\left(\Psi_N\left(\frac{R_1(\vartheta_i+1)}{2}\right)\right)} \gamma\left(\Psi_N, \frac{\sqrt{\tilde{\gamma}\left(\frac{1}{tP_R} - \frac{\Lambda_R}{P_R}\right)}}{\Theta_N\left(\frac{R_1(\vartheta_i+1)}{2}\right)}\right)\right\}dt, \tag{76}
$$

where $\tilde{\gamma} = P_L N_0$. Finally, using again the Chebyshev-Gauss quadrature approximation, the EE of RIS-assisted system in near-field can be approximated as (19). This completes the proof of **Lemma 5**.

REFERENCES

[1] S. Dang, O. Amin, B. Shihada, and M.-S. Alouini, "What should 6G be?" *Nat. Electron.*, vol. 3, no. 1, pp. 20–29, Jan. 2020.

[2] T. J. Cui, M. Q. Qi, X. Wan, J. Zhao, and Q. Cheng, "Coding metamaterials, digital metamaterials and programmable metamaterials," *Light Sci. Appl.*, vol. 3, no. 10, p. e218, Oct. 2014.

[3] W. Tang *et al.*, "Wireless communications with programmable metasurface: New paradigms, opportunities, and challenges on transceiver design," *IEEE Wireless Commun.*, vol. 27, no. 2, pp. 180–187, Apr. 2020.

[4] L. Zhang *et al.*, "Space-time-coding digital metasurfaces," *Nat. Commun.*, vol. 9, no. 1, pp. 1–11, 2018.

[5] W. Tang *et al.*, "Wireless communications with reconfigurable intelligent surface: Path loss modeling and experimental measurement," 2019. [Online]. Available: arXiv:1911.05326.

[6] E. Basar, "Reconfigurable intelligent surface-based index modulation: A new beyond MIMO paradigm for 6G," *IEEE Trans. Commun.*, vol. 68, no. 5, pp. 3187–3196, May 2020.

[7] E. Basar, M. Di Renzo, J. De Rosny, M. Debbah, M.-S. Alouini, and R. Zhang, "Wireless communications through reconfigurable intelligent surfaces," *IEEE Access*, vol. 7, pp. 116753–116773, 2019.

[8] J. Chen, Y.-C. Liang, H. V. Cheng, and W. Yu, "Channel estimation for reconfigurable intelligent surface aided multi-user MIMO systems," 2019. [Online]. Available: arXiv:1912.03619.

[9] Q.-U.-A. Nadeem, A. Kammoun, A. Chaaban, M. Debbah, and M.-S. Alouini, "Asymptotic max–min SINR analysis of reconfigurable intelligent surface assisted MISO systems," Dec. 2019. [Online]. Available: arXiv:1903.08127.

[10] Q.-U.-A. Nadeem, A. Kammoun, A. Chaaban, M. Debbah, and M.-S. Alouini, "Asymptotic max–min SINR analysis of reconfigurable intelligent surface assisted MISO systems," *IEEE Trans. Wireless Commun.*, vol. 19, no. 12, pp. 7748–7764, Dec. 2020.

[11] L. Subrt and P. Pechac, "Controlling propagation environments using intelligent walls," in *Proc. 6th Eur. Conf. Antennas Propag. (EUCAP)*, Prague, Czech, Jun. 2012, pp. 1–5.

[12] X. Xiong *et al.*, "Customizing indoor wireless coverage via 3D-fabricated reflectors," in *Proc. 4th ACM Int. Conf. Syst. Energy-Efficient Built Environ.*, Delft, The Netherlands, 2017, pp. 1–10.

[13] Y. Han, W. Tang, S. Jin, C.-K. Wen, and X. Ma, "Large intelligent surface-assisted wireless communication exploiting statistical CSI," *IEEE Trans. Veh. Technol.*, vol. 68, no. 8, pp. 8238–8242, Aug. 2019.

[14] C. Huang, R. Mo, and C. Yuen, "Reconfigurable intelligent surface assisted multiuser MISO systems exploiting deep reinforcement learning," 2020. [Online]. Available: arXiv:2002.10072.

[15] J. Ye, S. Guo, and M.-S. Alouini, "Joint reflecting and precoding designs for SER minimization in reconfigurable intelligent surfaces assisted MIMO systems," *IEEE Trans. Wireless Commun.*, vol. 19, no. 8, pp. 5561–5574, Aug. 2020.

[16] S. Guo, S. Lv, H. Zhang, J. Ye, and P. Zhang, "Reflecting modulation," *IEEE J. Sel. Areas Commun.*, vol. 38, no. 11, pp. 2548–2561, Nov. 2020.

[17] X. Yu, D. Xu, and R. Schober, "Enabling secure wireless communications via intelligent reflecting surfaces," in *Proc. IEEE Global Commun. Conf. (GLOBECOM)*, Waikoloa, HI, USA, 2019, pp. 1–6.

[18] C. Huang, G. C. Alexandropoulos, A. Zappone, M. Debbah, and C. Yuen, "Energy efficient multi-user MISO communication using low resolution large intelligent surfaces," in *Proc. IEEE Globecom Workshops (GC Wkshps)*, Abu Dhabi, UAE, Dec. 2018, pp. 1–6.

[19] W. Zhao, G. Wang, S. Atapattu, T. A. Tsiftsis, and C. Tellambura, "Is backscatter link stronger than direct link in reconfigurable intelligent surface-assisted system?" *IEEE Commun. Lett.*, vol. 24, no. 6, pp. 1342–1346, Jun. 2020.

[20] S. Atapattu, R. Fan, P. Dharmawansa, G. Wang, J. Evans, and T. A. Tsiftsis, "Reconfigurable intelligent surface assisted two-way communications: Performance analysis and optimization," 2020. [Online]. Available: arXiv:2001.07907.

[21] I. Trigui, W. Ajib, and W.-P. Zhu, "A comprehensive study of reconfigurable intelligent surfaces in generalized fading," 2020. [Online]. Available: arXiv:2004.02922.

[22] Z. Abdullah, G. Chen, S. Lambotharan, and J. A. Chambers, "A hybrid relay and intelligent reflecting surface network and its ergodic performance analysis," *IEEE Wireless Commun. Lett.*, vol. 9, no. 10, pp. 1653–1657, Oct. 2020.

[23] A.-A. A. Boulogeorgos and A. Alexiou, "Performance analysis of reconfigurable intelligent surface-assisted wireless systems and comparison with relaying," *IEEE Access*, vol. 8, pp. 94463–94483, 2020.

[24] Q. Tao, J. Wang, and C. Zhong, "Performance analysis of intelligent reflecting surface aided communication systems," *IEEE Commun. Lett.*, vol. 24, no. 11, pp. 2464–2468, Nov. 2020.

[25] L. Bariah, S. Muhaidat, P. C. Sofotasios, F. E. Bouanani, O. A. Dobre, and W. Hamouda, "Large intelligent surface assisted non-orthogonal multiple access: Performance analysis," 2020. [Online]. Available: arXiv:2007.09611.

[26] E. Björnson and L. Sanguinetti, "Power scaling laws and near-field behaviors of massive MIMO and intelligent reflecting surfaces," *IEEE Open J. Commun. Soc.*, vol. 1, pp. 1306–1324, 2020.

[27] E. Bjornson, O. Özdogan, and E. G. Larsson, "Intelligent reflecting surface versus decode-and-forward: How large surfaces are needed to beat relaying?" *IEEE Wireless Commun. Lett.*, vol. 9, no. 2, pp. 244–248, Feb. 2020.

[28] Q. Wu and R. Zhang, "Intelligent reflecting surface enhanced wireless network via joint active and passive beamforming," *IEEE Trans. Wireless Commun.*, vol. 18, no. 11, pp. 5394–5409, Nov. 2019.

[29] J. Lyu and R. Zhang, "Spatial throughput characterization for intelligent reflecting surface aided multiuser system," *IEEE Wireless Commun. Lett.*, vol. 9, no. 6, pp. 834–838, Jun. 2020.

[30] C. Huang, A. Zappone, G. C. Alexandropoulos, M. Debbah, and C. Yuen, "Reconfigurable intelligent surfaces for energy efficiency in wireless communication," *IEEE Trans. Wireless Commun.*, vol. 18, no. 8, pp. 4157–4170, Aug. 2019.

[31] L. Zhao, Z. Wang, and X. Wang, "Wireless power transfer empowered by reconfigurable intelligent surfaces," *IEEE Syst. J.*, early access, Apr. 28, 2020, doi: 10.1109/JSYST.2020.2985121.

[32] S. Sun, M. Fu, Y. Shi, and Y. Zhou, "Towards reconfigurable intelligent surfaces powered green wireless networks," 2020. [Online]. Available: arXiv:2005.01514.

[33] J. G. Andrews, "Seven ways that hetnets are a cellular paradigm shift," *IEEE Commun. Mag.*, vol. 51, no. 3, pp. 136–144, Mar. 2013.

[34] J. Hu and N. C. Beaulieu, "Performance analysis of decode-and-forward relaying with selection combining," *IEEE Commun. Lett.*, vol. 11, no. 6, pp. 489–491, Jun. 2007.

[35] A. Zappone, M. Di Renzo, F. Shams, X. Qian, and M. Debbah, "Overhead-aware design of reconfigurable intelligent surfaces in smart radio environments," 2020. [Online]. Available: arXiv:2003.02538.

[36] S. Atapattu, C. Tellambura, and H. Jiang, "A mixture Gamma distribution to model the SNR of wireless channels," *IEEE Trans. Wireless Commun.*, vol. 10, no. 12, pp. 4193–4203, Dec. 2011.

[37] I. S. Gradshteyn and I. M. Ryzhik, *Table of Integrals, Series, and Products*. Waltham, MA, USA: Academic, 2014.

[38] A. P. Prudnikov, J. A. Bryčkov, and O. I. Maričev, *Integrals and Series. Vol. 3, More Special Functions*, New York, NY, USA: Gordon Breach, 2003.

[39] V. S. Adamchik and O. I. Marichev, "The algorithm for calculating integrals of hypergeometric type functions and its realization in reduce system," in *Proc. Int. Symp. Symb. Algebraic Comput.*, Tokyo, Japan, Aug. 1990, pp. 212–224.

[40] G. Pan, Y. Chen, and Q. Feng, "Performance analysis of interference-limited cooperative systems with relay selection over independent log-normal fading channels," *IET Commun.*, vol. 8, no. 10, pp. 1751–1761, Jul. 2014.

[41] N. Ben Rached, Z. Botev, A. Kammoun, M.-S. Alouini, and R. Tempone, "On the sum of order statistics and applications to wireless communication systems performances," *IEEE Trans. Wireless Commun.*, vol. 17, no. 11, pp. 7801–7813, Nov. 2019.

[42] Q. Liu, T. Lv, and Z. Lin, "Energy-efficient transmission design in cooperative relaying systems using NOMA," *IEEE Commun. Lett.*, vol. 22, no. 3, pp. 594–597, Mar. 2018.

[43] J. N. Laneman, D. N. C. Tse, and G. W. Wornell, "Cooperative diversity in wireless networks: Efficient protocols and outage behavior," *IEEE Trans. Inf. Theory*, vol. 50, no. 12, pp. 3062–3080, Dec. 2004.

JIA YE (Student Member, IEEE) was born in Chongqing, China. She received the B.Sc. degree in communication engineering from Southwest University, Chongqing, China, in 2018, and the M.S. degree from the King Abdullah University of Science and Technology, Saudi Arabia, in 2020, where she is currently pursuing the Ph.D. degree. Her main research interests include the performance analysis and modeling of wireless/wireless communication systems.

ABLA KAMMOUN (Member, IEEE) was born in Sfax, Tunisia. She received the Engineering degree in signal and systems from Tunisia Polytechnic School, La Marsa, and the master's and Ph.D. degrees in digital communications from Telecom Paris Tech (formerly, École Nationale Supérieure des Télécommunications). From 2010 to 2012, she was a Postdoctoral Researcher with the TSI Department, Telecom Paris Tech. She was with Supélec, Alcatel-Lucent Chair on Flexible Radio until 2013. She is currently a Research Scientist with KAUST. Her research interests include performance analysis of wireless communication systems, random matrix theory, and statistical signal processing.
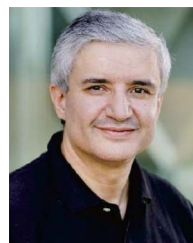
MOHAMED-SLIM ALOUINI (Fellow, IEEE) was born in Tunis, Tunisia. He received the Ph.D. degree in electrical engineering from the California Institute of Technology, Pasadena, CA, USA, in 1998. He served as a Faculty Member with the University of Minnesota, Minneapolis, MN, USA, then with the Texas A&M University at Qatar, Doha, Qatar, before joining the King Abdullah University of Science and Technology, Thuwal, Saudi Arabia, as a Professor of Electrical Engineering in 2009. His current research interests include the modeling, design, and performance analysis of wireless communication systems.